STEM CELLS AND DEVELOPMENT
Volume 23, Number 18, 2014

DOI: 10.1089/scd.2014.0200

GUEST EDITORIAL

Stem Cell Research and Regenerative Medicine in 2014: First Year of Regenerative Medicine in Japan

Hideyuki Okano

It is my great pleasure to announce that we were able to publish the Japan Issue in *Stem Cells and Development*, especially in this year 2014. This year, 2014, is said to be the First Year of Regenerative Medicine in Japan. This movement is likely to be based on the establishment of a new law system regarding regenerative medicine (an Act for Ensuring the Safety of Regenerative Medicine or the so-called Regenerative Medicine Law) and the partial revision of the Pharmaceutical Affairs Law (PAL). Both laws will come into effect in 2014 in this country. These new law systems are expected to have a great impact on the facilitation of R&D related to regenerative medicine and stem cell biology. In the present Japan Issue, some excellent stem cell research in this country will be introduced to celebrate the First Year of Regenerative Medicine in Japan.

Such a positive trend at least stems from recent groundbreaking achievements in stem cell biology and regenerative medicine, including the establishment of induced pluripotent stem (iPS) cell technologies by Yamanaka and colleagues [1,2]. Notably, in 2014, Dr. Masayo Takahashi at the Laboratory for the Retinal Regeneration Project, Center for Developmental Biology, RIKEN, Japan, is going to start the first clinical trial using iPS cell-derived cell products. The Takahshi Group is aiming to transplant autologous iPS cell-derived retinal pigment epithelium sheets in patients suffering from wet-type age-related macular degeneration (AMD) [3]. Following this application for AMD, several clinical trials examining iPS cell-based cell therapy are currently being prepared for patients with Parkinson's disease, spinal cord injury, thrombocytopenia, myocardial infarction, and other diseases in Japan [4]. There is also increasing interest in modeling human diseases using iPS cell technologies, which could contribute to the future drug screening and preemptive medicine [5,6]. Considering these possibilities, iPS cell technologies are expected to open a new era, providing enormous opportunities in the field of biomedical research. However, needless to say, safety-related concerns for iPS cell-based cell therapy should be resolved before the clinical application of iPS cells in the field of regenerative medicine [7,8].

However, I wish to emphasize that iPS cell technology is not the sole advantage of Japanese stem cell science. As already summarized in the Theme Issue "Japan: Its Tradition and Hot Topics in Biological Sciences" in the *Philosophical Transaction of the Royal Society B* in 2008, stem cell biology has been described as a strong and exciting research field in Japan, together with single-molecule imaging and neuroscience [9]. Almost 150 years ago, when the Meiji period began, the Japanese government invited prominent European scientists to build the new so-called Imperial Universities to facilitate the nation's science and technology. Many of the prominent scientists who were invited included professors of developmental biology and embryology, which has resulted in the advantage of a long history in the training of talented human resources in this field in Japan [9]. On the other hand, regretfully, serious confusion and controversies appeared in 2014 regarding the new method of obtaining pluripotent cells through the exposure of somatic cells to sublethal stresses [10]. This new method and proposed concept for the stress-induced acquisition of pluripotency needs to be tested by third parties. Obviously, Japanese stem cell researchers need to overcome this unfavorable situation with solid experimental data and transparency in this memorable First Year of Regenerative Medicine in Japan.

In the present Japan Issue of this Journal, to celebrate the First Year of Regenerative Medicine in Japan, I wish to introduce some excellent stem cell research efforts in Japan, particularly in the following fields from the following laboratories:

1. Pluripotent stem cells and differentiation (Kosodo and colleagues [11]; Ohneda and colleagues [12]; Egusa et al. [13]; Okuda and colleagues [14]; Furue and colleagues [15]).
2. Somatic stem cells and progenitor cells and targeting of precancerous populations (Nishida and colleagues [16]; Kawabata and colleagues [17]; Moriyama et al. [18]; Wada et al. [19]; Taniguchi and colleagues [20]).
3. Molecular mechanism of transcriptional regulation and cell differentiation (Kawase et al. [21]).

Department of Physiology, Keio University School of Medicine, Tokyo, Japan.

I hope that you will enjoy this Special Issue of *Stem Cells and Development* and that this issue will lead to a wider appreciation of our nation's contribution to stem cell research and regenerative medicine.

Acknowledgments

This study was supported by grants from the Program for Intractable Disease Research Utilizing Disease-Specific iPS Cells and the Research Center Network for the Realization of Regenerative Medicine, funded by the Japan Science and Technology Agency (JST) to H.O.

Author Disclosure Statement

H.O. is a paid scientific consultant at San Bio, Co. Ltd., and Daiichi Sankyo Co., Ltd.

References

1. Takahashi K and S Yamanaka. (2006). Induction of pluripotent stem cells from mouse embryonic and adult fibroblast cultures by defined factors. Cell 7:663–676.
2. Takahashi K, K Tanabe, M Ohnuki, M Narita, T Ichisaka, K Tomoda and S Yamanaka. (2007). Induction of pluripotent stem cells from adult human fibroblasts by defined factors. Cell 7:861–872.
3. Kamao H, M Mandai, S Okamoto, N Sakai, A Suga, SJ Sugita, JM Kiryu and M Takahashi. (2014). Characterization of human induced pluripotent stem cell-derived retinal pigment epithelium cell sheets aiming for clinical application. Stem Cell Rep 7:1–14.
4. Okano H and S Yamanaka. (2014). iPS cell technologies: significance and applications to CNS regeneration and disease. Mol Brain 7:22.
5. Mattis VB and CN Svendsen. (2011). Induced pluripotent stem cells: a new revolution for clinical neurology? Lancet Neurol 10:383–394.
6. Imaizumi Y and H Okano. (2013). Modeling human neurological disorders with induced pluripotent stem cells. J Neurochem 129:388–399.
7. Nakamura M and H Okano. (2013). Cell transplantation therapies for spinal cord injury focusing on induced pluripotent stem cells. Cell Res 23:70–80.
8. Okano H, M Nakamura, K Yoshida, Y Okada, O Tsuji, S Nori, E Ikeda, S Yamanaka and K Miura. (2013). Steps toward safe cell therapy using induced pluripotent stem cells. Circ Res 112:523–533.
9. Okano H, T Yanagida and A Iriki. (2008). Introduction. Japan: its tradition and hot topics in biological sciences. Philos Trans R Soc Lond B Biol Sci 363:2067–2069.
10. Cyranoski D. (2014). Stem-cell method faces fresh questions. Nature 507:283.
11. Nagashima F, IK Suzuki, A Shitamukai, H Sakaguchi, M Iwashita, T Kobayashi, S Tone, K Toida, P Vanderhaeghen and Y Kosodo. (2014). Novel and robust transplantation reveals the acquisition of polarized processes by cortical cells derived from mouse and human pluripotent stem cells. Stem Cells Dev 23:2129–2142.
12. Zhao Y, M Matsuo-Takasaki, I Tsuboi, K Kimura, GT Salazar, T Yamashita and O Ohneda. (2014). Dual functions of hypoxia inducible factor-1α for the commitment of mouse embryonic stem cells toward a neural lineage original research report. Stem Cells Dev 23:2143–2155.
13. Egusa H, H Kayashima, J Miura, S Uraguchi, F Wang, H Okawa, JI Sasaki, M Saeki, T Matsumoto and H Yatani. (2014). Comparative analysis of mouse induced pluripotent stem cells and mesenchymal stem cells during osteogenic differentiation in vitro. Stem Cells Dev 23:2156–2169.
14. Kamon M, M Katano, K Hiraki-Kamon, T Hishida, Y Nakachi, Y Mizuno, Y Okazaki, A Suzuki, M Hirasaki, et al. (2013) Identification of Ccr4-not complex components as regulators of transition from partial to genuine induced pluripotent stem cells. Stem Cells Dev 23:2170–2179.
15. Kinehara M, S Kawamura, S Mimura, M Suga, A Hamada, M Wakabayashi, H Nikawa and MK Furue. (2014) Protein kinase C-induced early growth response protein-1 binding to SNAIL promoter in epithelial-mesenchymal transition of human embryonic stem cell. Stem Cells Dev 23:2180–2189.
16. Hara S, R Hayashi, T Soma, T Kageyama, T Duncan, M Tsujikawa and K Nishida. (2014). Identification and potential application of human corneal endothelial progenitor cells. Stem Cells Dev 23:2190–2201.
17. Tashiro K, A Nonaka, N Hirata, T Yamaguchi, H Mizuguchi and K Kawabata. (2014). Plasma elevation of vascular endothelial growth factor leads to the reduction of mouse hematopoietic and mesenchymal stem/progenitor cells in the bone marrow. Stem Cells Dev 23:2202–2210.
18. Moriyama M, H Isshi, S Ishihara, H Okura, A Ichinose, T Ozawa, A Matsuyama and T Hayakawa. (2014). Role of Notch signaling in the maintenance of human mesenchymal stem cells under hypoxic conditions. Stem Cells Dev 23:2211–2224.
19. Wada N, H Maeda, D Hasegawa, S Gronthos, PM Bartold, D Menicanin, S Fujii, S Yoshida, A Tomokiyo, S Monnouchi and A Akamine. (2014). Semaphorin 3A induces mesenchymal stem-like properties in human periodontal ligament cells. Stem Cells Dev 23:2225–2236.
20. Zheng YW, T Tsuchida, T Shimao, B Li, T Takebe, RR Zhang, Y Sakurai, Y Ueno, K Sekine, et al. (2014). The CD133+CD44+ precancerous subpopulation of oval cells is a therapeutic target for hepatocellular carcinoma. Stem Cells Dev 23:2237–2249.
21. Kawase S, K Kuwako, T Imai, F Renault-Mihara, K Yaguchi, S Itohara and H Okano. (2014). Rfx transcription factors control musashi1 transcription in mouse neural stem/progenitor cells. Stem Cells Dev 23:2250–2261.

Address correspondence to:
Dr. Hideyuki Okano
Department of Physiology
Keio University School of Medicine
35 Shinanomachi
Shinjuku
Tokyo 160-8582
Japan

E-mail: hidokano@a2.keio.jp

interesting since the adult pancreas lacks progenitor cells (Dor et al., 2004).

To investigate which SCF^{Fbxw7} substrates may play a role during β cell emergence in the *Fbxw7*-deleted pancreas, the authors analyzed a panel of four transcription factors known to be involved in embryonic β cell development and found that both the mRNA and protein levels of Ngn3, but not those of the other three, were strongly increased in *Fbxw7*-deleted pancreas. They then demonstrated that knockdown of Fbxw7 reduced Ngn3 ubiquitination and increased Ngn3 protein half-life. Fbxw7 binds to Ngn3 and this binding, like the interactions between many other F-box proteins and their substrates, requires the GSK3β-mediated phosphorylation of Ngn3 on two adjacent serine residues, a characteristic feature of phosphodegron motifs. Conditional transgenic expression of a phosphodegron mutant Ngn3, in the presence of endogenously expressed Fbxw7, quickly (within 24 hr) resulted in the emergence of insulin-positive β cells in the pancreas. Together with the results from the pancreas-conditional deletion of *Fbxw7*, these findings suggest that the β cells arise through direct conversion of ductal cells rather than an intermediate progenitor cell that divides prior to differentiation (Sancho et al., 2014).

Aside from identifying Fbxw7 as a regulator of cell fate decision in both embryonic and adult pancreas and showing an example of direct ductal-to-β cell conversion, the study offers new evidence consistent with the lack of stem/progenitor cells in the adult pancreas. It also highlights the latent plasticity of mature adult cells, which are generally viewed as terminally differentiated. However, there are two important issues that remain to be determined. First, unlike most other E3 substrates whose mRNA levels remain largely unchanged when the E3 function is disrupted, the mRNA level of *Ngn3* is also increased in *Fbxw7*-deleted cells. Although the authors propose a positive feedback loop to explain this perplexing phenomenon, both the direct evidence supporting this loop and its significance are yet to be demonstrated. Second, Fbxw7 also degrades several additional proteins that play a critical role in regulating cell growth, proliferation, and fate (Figure 1). Whether these proteins are also regulated by Fbxw7 in the embryonic and adult pancreas has not been examined. Does Fbxw7 control β cell neogenesis solely through Ngn3 or through coordinated regulation of multiple substrates? Ultimately, the in vivo induction of functional β cells may be a viable treatment option for patients with type 1 diabetes mellitus, and the current finding of the $SCF/CRL1^{Fbxw7}$-Ngn3 axis in controlling direct ductal-to-β cell conversion offers a new target for this exploration.

ACKNOWLEDGMENTS

We thank Menxi Liu for helping with figure preparation. Y.X. is supported by NIH grant GM067113.

REFERENCES

Atkinson, M.A., Bluestone, J.A., Eisenbarth, G.S., Hebrok, M., Herold, K.C., Accili, D., Pietropaolo, M., Arvan, P.R., Von Herrath, M., Markel, D.S., and Rhodes, C.J. (2011). Diabetes *60*, 1370–1379.

Dor, Y., Brown, J., Martinez, O.I., and Melton, D.A. (2004). Nature *429*, 41–46.

Edlund, H. (2002). Nat. Rev. Genet. *3*, 524–532.

Inada, A., Nienaber, C., Katsuta, H., Fujitani, Y., Levine, J., Morita, R., Sharma, A., and Bonner-Weir, S. (2008). Proc. Natl. Acad. Sci. USA *105*, 19915–19919.

Pagliuca, F.W., and Melton, D.A. (2013). Development *140*, 2472–2483.

Pickart, C.M. (2001). Annu. Rev. Biochem. *70*, 503–533.

Sancho, R., Gruber, R., Gu, G., and Behrens, A. (2014). Cell Stem Cell *15*, this issue, 139–153.

Welcker, M., and Clurman, B.E. (2008). Nat. Rev. Cancer *8*, 83–93.

Zhou, Q., Brown, J., Kanarek, A., Rajagopal, J., and Melton, D.A. (2008). Nature *455*, 627–632.

Leptin Receptor Makes Its Mark on MSCs

Yumi Matsuzaki,[1] Yo Mabuchi,[2,3] and Hideyuki Okano[3,*]
[1]Department of Life Science Laboratory of Tumor Biology, Shimane University Faculty of Medicine, Izumo, Shimane 693-8501, Japan
[2]Department of Biochemistry and Biophysics, Graduate School of Health Care Sciences, Tokyo Medical and Dental University, Bunkyo-ku, Tokyo 113-8510, Japan
[3]Department of Physiology, Keio University School of Medicine, Shinjuku-ku, Tokyo 160-8582, Japan
*Correspondence: hidokano@a2.keio.jp
http://dx.doi.org/10.1016/j.stem.2014.07.001

Although mesenchymal stem/stromal cells (MSCs) are an important component of the hematopoietic niche, the markers that correlate with their physiological functions have not been defined. In this issue of *Cell Stem Cell*, Zhou et al. (2014) identify the Leptin Receptor as a marker for prospective identification and in vivo fate mapping of bone marrow MSCs.

Mesenchymal stem/stromal cells (MSCs) have been defined as nonhematopoietic, plastic-adherent, colony-forming cells that are capable of in vitro trilineage differentiation into fat, bone, and cartilage (Pittenger et al., 1999). While MSCs can be retrospectively identified based on their ability to produce colony-forming unit fibroblasts (CFU-Fs) in vitro, an

appropriate method for their prospective identification was lacking until very recently, and their location and physiological functions in vivo have been elusive.

The lack of unique markers and discrepancies arising from the use of different lineage tracing mouse strains has contributed to the confusion facing this field in the past. The turning point in the study of MSC markers was the identification of PDGFRα as a mesenchymal stem cell marker. Mouse MSCs are highly concentrated in the CD45$^-$Ter119$^-$PDGFRα$^+$Sca-1$^+$ (PαS) population (Morikawa et al., 2009a). In addition, PDGFRα$^+$Sca-1$^-$ cells were found to secrete CXCL12 in the same manner as CXCL12-abundant reticular (CAR) cells, which are a key component of the niche for hematopoietic stem cells (HSCs) in adult bone marrow (BM) (Omatsu et al., 2014). One report defined *Nestin*-GFP$^+$ cells in the BM as "mesensphere"-forming cells that are required for maintenance and homing of HSCs (Méndez-Ferrer et al., 2010). Conversely, another group reported that *Nestin*-GFP$^+$ cells were rarely CFU-F cells and were often non-MSC populations (Ding et al., 2012). Therefore, it is likely that the *Nestin*-GFP$^+$ and PαS populations partially overlap but are mostly distinct.

In this issue of *Cell Stem Cell*, Morrison and colleagues identify the Leptin Receptor (LepR), a receptor for a fat-cell-specific hormone that was expressed in approximately 0.3% of BM cells (Zhou et al., 2014), as an excellent marker for the prospective identification of mouse MSCs. Notably, 10% of LepR$^+$ cells are CFU-Fs, and they account for the vast majority (94%) of CFU-Fs in adult mouse BM. Furthermore, LepR$^+$ cells in the limb BM were uniformly positive for the MSC marker Prx1.

This group also showed that LepR$^+$ stromal and CAR cells, which are located primarily around the sinusoids, are found in a largely overlapping region (Omatsu et al., 2010). They showed that LepR$^+$ cells were *Nestin*-GFP^{low}. However, these cells were negative for a *Nestin*-Cre^{ER}-labeled marker (*Nestin*-Cre^{ER}; loxp-EYFP). This inconsistency can be interpreted as follows: *Nestin*-GFP^{low}, in which GFP is regulated by the second intronic enhancer of the *Nestin* gene, was reported to serve as a marker for mesenchymal cells (Méndez-Ferrer et al., 2010). However, *Nestin*-GFP expression levels are not very high in MSCs, in contrast to strong expression in neural stem/progenitor cells, where expression is putatively mediated by the action of Brn2 and Sox2 on the *Nestin* second intronic enhancer (Sunabori et al., 2008). To our knowledge, transcription factors acting on this enhancer have not yet been identified in MSCs. Furthermore, GFP is not knocked into the endogenous *Nestin* gene in this model. Instead, its expression is driven from a transgene inserted into a chromosome. Thus, the *Nestin*-GFP expression profile is likely to be variable between the various *Nestin*-GFP transgenic mouse lines. This variability can account for the different overlapping patterns between LepR and *Nestin*-GFP^{low} or *Nestin*-Cre^{ER}; loxp-EYFP in the present study (Zhou et al., 2014). Based on these findings, researchers should carefully select *Nestin* transgenic lines to mark MSCs.

As for Cre^{ER}-mediated lineage tracing experiments, it is important to appreciate that different regimens of tamoxifen could produce different results. Thus, in order to label MSCs using *Nestin* transgenic lines, it is important to use the appropriate transgenic reporter line and an appropriate induction regimen that guarantees robust recombination. The Nestin protein expression profile is more complicated than the *Nestin*-driven transgene expression because the mesoderm-specific first intronic enhancer is involved in endogenous *Nestin* gene expression. However, fortunately for MSC researchers, LepR-immunopositive cells are also almost always *Lepr*-Cre-labeled cells in BM stroma (Zhou et al., 2014), indicating that LepR is a reliable and versatile MSC marker. Figure 1 illustrates the relationships between various MSC markers in an effort to synthesize findings from the present and previous reports.

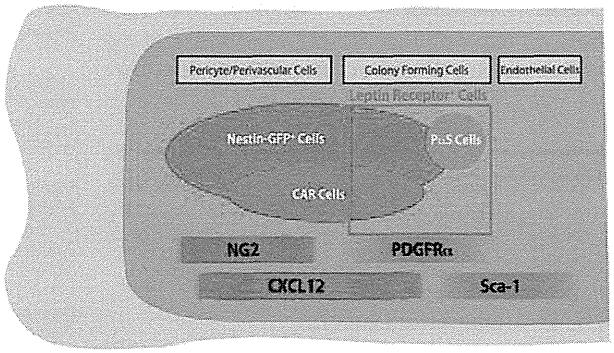

Figure 1. Correlation between LepR$^+$ Cells and Distinct Mesenchymal Markers in Bone Marrow

PDGFRα cells are derived from adult bone marrow cells that can be marked by LepR. LepR$^+$ cells include Sca-1$^-$ and Sca-1$^+$ cells. PDGFRα$^+$Sca-1$^+$ cells, which are PαS cells, are high efficiently CFU-F-forming cells. Conversely, PDGFRα$^+$Sca-1$^-$ cells secrete significant levels of CXCL12 and are a subgroup of the CAR cells. There is a small portion of the PαS, CAR, and LepR$^+$ cells that overlaps with the *Nestin*-GFP^{low} (Low) cells, which are widely expressed in many types of cells. MSC, mesenchymal stem cell; CAR cells, CXCL12 (a chemokine)-abundant reticular cells.

Furthermore, Zhou et al. (2014) performed an excellent fate mapping study of LepR$^+$ cells. Using *Lepr*-Cre/loxp-mediated lineage tracing, they showed that during ontogenic development, LepR$^+$ cells appear postnatally in the BM and are a major source of new osteoblasts and adipocytes in adult BM. As for the developmental origin of MSCs, previous studies have shown that prospective isolation of adult mouse BM MSCs positive for PαS included *Wnt1*-Cre- and *P0*-Cre-labeled, neural-crest-marker-positive, neurosphere-initiating units (Morikawa et al., 2009b), which can also give rise to neurons, glial cells, and myofibroblasts. Furthermore, Morikawa et al. showed that CFU-Fs were included in the *P0*-Cre-labeled and nonlabeled PαS cells at a very similar frequency, indicating that cells of the neural crest origin could contribute to MSCs in adult mouse BM. Conversely, Zhou et al. (2014) surprisingly found that *Wnt1*-Cre-labeled neural crest cells rarely included CFU-Fs and thus are likely to be a distinct population from the LepR$^+$ BM cells. These discrepancies could result from differences in the transgenic Cre lines used to mark neural crest cells or differences in other experimental conditions. In any case, it would be interesting to test whether a single MSC that has both

CFU-F activity and neural crest characteristics is present in adult mouse BM.

It is notable that LepR, a hormone receptor, is a marker of MSCs and that LepR$^+$ cells are involved in the regenerative response of bone and cartilage after injury. Thus, an attractive idea is that the fat-cell-specific hormone Leptin and the LepR/Jak/STAT pathway, which is blocked in *db/db* mice, play crucial roles in the biological regulation (e.g., maintenance, proliferation, and/or differentiation) of MSCs and the regenerative responses of bone and cartilage. Thus, the paracrine action of Leptin released from BM adipocytes to the LepR$^+$ MSCs could possibly be involved in the homeostasis of MSCs and MSCs-derived cells, which should be elucidated in future investigations.

The study of MSCs is likely to have both biological significance and clinical applications. In human MSCs, enriched expression of the low-affinity nerve growth factor receptor (LNGFR) (known as a neural crest marker) has been reproduced by many researchers (Mabuchi et al., 2013), but the consistency of the marker remains a problem. The next step should be conducting comprehensive analysis using LepR in multiple species. By refining our ability to define MSCs in vivo, the field may then shift directions from markers to signaling and focus on establishing MSC biology in the near future.

ACKNOWLEDGMENTS

H.O. is a Founding Scientist and a paid SAB of San Bio Co. Ltd.

REFERENCES

Ding, L., Saunders, T.L., Enikolopov, G., and Morrison, S.J. (2012). Nature *481*, 457–462.

Mabuchi, Y., Morikawa, S., Harada, S., Niibe, K., Suzuki, S., Renault-Mihara, F., Houlihan, D.D., Akazawa, C., Okano, H., and Matsuzaki, Y. (2013). Stem Cell Reports *1*, 152–165.

Méndez-Ferrer, S., Michurina, T.V., Ferraro, F., Mazloom, A.R., Macarthur, B.D., Lira, S.A., Scadden, D.T., Ma'ayan, A., Enikolopov, G.N., and Frenette, P.S. (2010). Nature *466*, 829–834.

Morikawa, S., Mabuchi, Y., Kubota, Y., Nagai, Y., Niibe, K., Hiratsu, E., Suzuki, S., Miyauchi-Hara, C., Nagoshi, N., Sunabori, T., et al. (2009a). J. Exp. Med. *206*, 2483–2496.

Morikawa, S., Mabuchi, Y., Niibe, K., Suzuki, S., Nagoshi, N., Sunabori, T., Shimmura, S., Nagai, Y., Nakagawa, T., Okano, H., and Matsuzaki, Y. (2009b). Biochem. Biophys. Res. Commun. *379*, 1114–1119.

Omatsu, Y., Sugiyama, T., Kohara, H., Kondoh, G., Fujii, N., Kohno, K., and Nagasawa, T. (2010). Immunity *33*, 387–399.

Omatsu, Y., Seike, M., Sugiyama, T., Kume, T., and Nagasawa, T. (2014). Nature *508*, 536–540.

Pittenger, M.F., Mackay, A.M., Beck, S.C., Jaiswal, R.K., Douglas, R., Mosca, J.D., Moorman, M.A., Simonetti, D.W., Craig, S., and Marshak, D.R. (1999). Science *284*, 143–147.

Sunabori, T., Tokunaga, A., Nagai, T., Sawamoto, K., Okabe, M., Miyawaki, A., Matsuzaki, Y., Miyata, T., and Okano, H. (2008). J. Cell Sci. *121*, 1204–1212.

Zhou, B.O., Yue, R., Murphy, M.M., Peyer, J.G., and Morrison, S.J. (2014). Cell Stem Cell *15*, this issue, 154–168.

The Tailless Root of Glioma: Cancer Stem Cells

Qi Xie,[1] William A. Flavahan,[1] Shideng Bao,[1] and Jeremy Rich[1,*]
[1]Department of Stem Cell Biology and Regenerative Medicine, Lerner Research Institute, Cleveland, OH 44195, USA
*Correspondence: drjeremyrich@gmail.com
http://dx.doi.org/10.1016/j.stem.2014.07.004

In this issue of *Cell Stem Cell*, Zhu et al. (2014) demonstrate that a genetically engineered glioma model displays a functional cellular hierarchy defined by expression of the nuclear orphan receptor Tlx. Targeting cancer stem cells through genetic deletion of TLX promotes cancer stem cell death and differentiation and extends survival.

Cancer is a genetic disease, but it initiates and grows within a cellular context that reflects the organization of tumors into aberrant organ systems. The cellular diversity within a tumor extends to the neoplastic compartment in which genetic and epigenetic variation manifests in differential proliferation, survival, and migration of cancer cells. The cancer stem cell (CSC) hypothesis is a partial explanation for these observations because many cancers harbor a relatively undifferentiated pool of transformed cells that self-renew and propagate the entire range of differentiated tumor progeny. However, establishing the presence of cellular hierarchies within a tumor and identifying the origin of differentiated progeny is complicated by the dynamic nature of cancer and an inability to trace the history of existing cancers. One challenge has been the identification of reliable CSC surface markers because these molecules mediate interactions between cells and their microenvironment and may be dynamically changed after isolation of CSCs. Further, no tumor type is genetically uniform, so markers are unlikely to be uniformly informative in all tumors. Tumor models derived from patient specimens (e.g., patient-derived xenografts) contain the cellular and molecular diversity of the human disease but cannot instruct us as to the natural history of specific cells beyond genetic lineage analysis. Alternatively, genetically engineered mouse models present a useful tool to study the natural history of tumor hierarchies in an immune-competent

Stem Cell Reports
Article

OPEN ACCESS

Involvement of ER Stress in Dysmyelination of Pelizaeus-Merzbacher Disease with *PLP1* Missense Mutations Shown by iPSC-Derived Oligodendrocytes

Yuko Numasawa-Kuroiwa,[1,2] Yohei Okada,[1,3,*] Shinsuke Shibata,[1] Noriyuki Kishi,[1] Wado Akamatsu,[1] Masanobu Shoji,[4] Atsushi Nakanishi,[4] Manabu Oyama,[5] Hitoshi Osaka,[6] Ken Inoue,[7] Kazutoshi Takahashi,[8] Shinya Yamanaka,[8] Kenjiro Kosaki,[9] Takao Takahashi,[2] and Hideyuki Okano[1,*]

[1]Department of Physiology, School of Medicine, Keio University, 35 Shinanomachi, Shinjuku-ku, Tokyo 160-8582, Japan
[2]Department of Pediatrics, School of Medicine, Keio University, 35 Shinanomachi, Shinjuku-ku, Tokyo 160-8582, Japan
[3]Department of Neurology, School of Medicine, Aichi Medical University, 1-1 Yazako Karimata, Nagakute, Aichi 480-1195, Japan
[4]Advanced Science Research Laboratories, Takeda Pharmaceutical Company Limited, 26-1 Muraoka-Higashi 2-Chome, Fujisawa, Kanagawa 251-8555, Japan
[5]Department of Dermatology, School of Medicine, Keio University, 35 Shinanomachi, Shinjuku-ku, Tokyo 160-8582, Japan
[6]Department of Pediatrics, Jichi Medical School, 3311-1 Yakushiji, Shimotsuke-shi, Tochigi 329-0498, Japan
[7]Department of Mental Retardation and Birth Defect Research, National Institute of Neuroscience, National Center of Neurology and Psychiatry, 4-1-1 Ogawahigashi-machi, Kodaira-shi, Tokyo 187-8551, Japan
[8]Center for Induced Pluripotent Stem Cell Research and Application, Graduate School of Medicine, Institute for Frontier Medical Sciences, Kyoto University, Kyoto 606-8507, Japan
[9]Center for Medical Genetics, School of Medicine, Keio University, 35 Shinanomachi, Shinjuku-ku, Tokyo 160-8582, Japan
*Correspondence: yohei@a6.keio.jp (Y.O.), hidokano@a2.keio.jp (H.O.)
http://dx.doi.org/10.1016/j.stemcr.2014.03.007

SUMMARY

Pelizaeus-Merzbacher disease (PMD) is a form of X-linked leukodystrophy caused by mutations in the *proteolipid protein 1* (*PLP1*) gene. Although PLP1 proteins with missense mutations have been shown to accumulate in the rough endoplasmic reticulum (ER) in disease model animals and cell lines transfected with mutant *PLP1* genes, the exact pathogenetic mechanism of PMD has not previously been clarified. In this study, we established induced pluripotent stem cells (iPSCs) from two PMD patients carrying missense mutation and differentiated them into oligodendrocytes in vitro. In the PMD iPSC-derived oligodendrocytes, mislocalization of mutant PLP1 proteins to the ER and an association between increased susceptibility to ER stress and increased numbers of apoptotic oligodendrocytes were observed. Moreover, electron microscopic analysis demonstrated drastically reduced myelin formation accompanied by abnormal ER morphology. Thus, this study demonstrates the involvement of ER stress in pathogenic dysmyelination in the oligodendrocytes of PMD patients with the *PLP1* missense mutation.

INTRODUCTION

Analysis of differentiated cells from disease-specific, human induced pluripotent stem cells (iPSCs) enables the construction of pathological models using the patients' own cells. Such analyses are particularly useful for the study of neurodegenerative disorders because it is difficult to collect brain-tissue samples from these patients.

Pelizaeus-Merzbacher disease (PMD) is a dysmyelinating disorder of the CNS that is usually observed during childhood. PMD is classified into two subtypes: the classical and connatal forms. In the classical form, patients usually show a delay in psychomotor development within the first year of life but exhibit relatively slow disease progression over the first decade. In contrast, in the connatal form, patients generally show arrested congenital psychomotor development and exhibit a progressive disease course with severe neurological impairment. The degree of dysmyelination has been shown to correlate well with the clinical severity of PMD (Seitelberger, 1995). The *proteolipid protein 1* (*PLP1*) gene has been identified as a causative gene for PMD. PLP1 is a transmembrane protein that is abundantly expressed in compact myelin in oligodendrocytes (OLs) and plays a structural role in the formation and maintenance of myelin sheaths (Gow et al., 1997; Mikoshiba et al., 1991). Three distinct types of *PLP1* mutation have been reported to date: point mutations, duplications, and deletions. Missense mutations in the *PLP1* gene account for 30% of the genetic abnormalities found in PMD patients and are responsible for most of connatal cases. Based on analyses using cell lines transfected with mutant *PLP1* genes (Gow and Lazzarini, 1996) or a mouse model of PMD (the *msd* mouse; Gow et al., 1998), the underlying pathogenesis in most patients with missense mutations is thought to involve the accumulation of misfolded mutant PLP1 proteins in the rough endoplasmic reticulum (ER) (Southwood et al., 2002) and the induction of ER stress, resulting in activation of the unfolded protein response (UPR). Although UPR attenuates general translation to reduce the protein load into ER and increase expression of chaperone proteins to facilitate protein folding, excessive levels of unfolded proteins have been shown to activate apoptotic pathway of UPR to eliminate damaged OLs.

However, despite the precise analyses conducted using conventional cellular and animal PMD models, it has not been possible to examine the actual correlation between the known molecular pathogenesis and cell biological phenotypes, including abnormalities in OL differentiation, myelination, and cell death. In addition, those previous results were obtained through analyses using nonhuman models, non-patient-derived cells, or nonoligodendrocyte models, and it is unknown whether the results obtained in those models are applicable to human patients. Although the establishment of iPSCs from a PMD patient with partial duplication of *PLP1* gene has been reported, those iPSCs were not differentiated into oligodendrocytes for disease modeling (Shimojima et al., 2012). Thus, in the present study, we focused on the pathologic effects of *PLP1* missense mutations and established patient-specific iPSCs from two PMD patients with different mutation sites and different levels of clinical severity.

We differentiated the iPSCs into OL lineage cells and examined the pathogenic changes in the PMD iPSC-derived OLs. We confirmed the accumulation and mislocalization of mutant PLP1 proteins to the ER, a high level of stress susceptibility, and increased apoptosis in PMD iPSC-derived OLs. In addition, through transmission electron microscopic analysis, we verified decreases in the frequency of myelin formation and the thickness of the myelin sheath compared with control cells. More importantly, we also demonstrated that these pathogenic changes observed in iPSC-derived OLs were consistent with the different levels of clinical severity between the two PMD patients. Thus, this report describes the modeling of human PMD with *PLP1* missense mutations using patient-specific, iPSC-derived OLs. These results have demonstrated the usefulness of iPSC-derived OLs for the analysis of the pathogenic processes in human dysmyelinating neurological disorders.

RESULTS

Clinical Features of PMD Patients

We established iPSCs from two patients with point mutations in the transmembrane domain (patient 1: PMD1) and extracellular domain (patient 2: PMD2) of the *PLP1* gene (Figure 1C). PMD1 was a 1-year-old male with the connatal form of PMD. He was diagnosed with PMD at the age of 4 months, when he was found to exhibit poor head control and nystagmus and was unable to follow objects. He showed poor feeding and was fed through a gastrostomy tube from the age of 21 months. Psychomotor development was not observed, even at the age of 5 years. MRI of the patient's brain revealed mild and diffuse atrophy, dilatation of the ventricles, and diffuse high-intensity signals in the white matter of the cerebrum and brainstem in a T2-weighted image (T2WI) (Figure 1A). A direct sequencing analysis of genomic DNA from the patient's leukocytes showed a novel missense mutation, c.757 T > A (p.Ser253Thr), in exon 6 of the *PLP1* gene (Figure 1B). This amino acid change has not been previously reported, but different type of mutation at this same site, Ser253Phe, has been reported in other patients with the connatal form of PMD (Hodes et al., 1998). This change was not identified in more than 200 normal individuals; thus, it was considered to be a causative mutation for PMD.

Patient 2 (PMD2) was a 20-year-old male with the classical form of PMD. He was diagnosed with PMD at the age of 3 months, when he was found to display poor head control and nystagmus. Spastic quadriparesis was evident at 4 years of age, with choreoathetotic movements beginning at the age of 8–10 years. He appeared alert and attentive and was nonverbal but exhibited guttural vocalizations. A missense mutation, c.643 C > T (p.Pro215Ser), was identified in exon 5 of the *PLP1* gene, which has been reported previously (Gencic et al., 1989).

Establishment and Characterization of iPSCs Derived from PMD Patients

Human iPSCs were established via the retroviral transduction of four transcription factors (*SOX2*, *OCT4*, *KLF4*, and *c-MYC*) into dermal fibroblasts (Takahashi et al., 2007). A total of 52 and 34 iPSC clones were established from PMD1 and PMD2 samples, respectively. The established iPSC clones were evaluated based on the typical morphology of colonies similar to human embryonic stem cells (ESCs), as well as the expression of pluripotent markers via immunocytochemistry (NANOG and OCT4; Figure 1D), silencing of retroviral transgenes through quantitative RT-PCR (Figure 1E), and efficient differentiation into neural cells via embryoid body (EB) formation. We finally selected three clones each for PMD1 (1-7, 1-15, and 1-27) and PMD2 (2-6, 2-10, and 2-22) for further analyses. The differentiation potentials of these selected iPSC clones were confirmed through teratoma formation assays (ectoderm: neural rosettes and pigmented epithelium, endoderm: goblet cells, and mesoderm: bones and cartilage; Figure 1F). Moreover, the mutations in the *PLP1* gene (PMD1 [c.757 T > A] and PMD2 [c.643 C > T]) were confirmed in human dermal fibroblasts (HDFs) and all of the selected iPSC clones via pyrosequencing analysis (Figure 1G).

Regarding the control iPSCs, we used age-matched control iPSCs established from 8-month-old (TIG121) and 16-year-old (WD39) healthy individuals, corresponding to the PMD-iPSCs established from 1-year-old and 20-year-old patients, respectively, as well as 201B7, which is a widely used control iPSC clone.

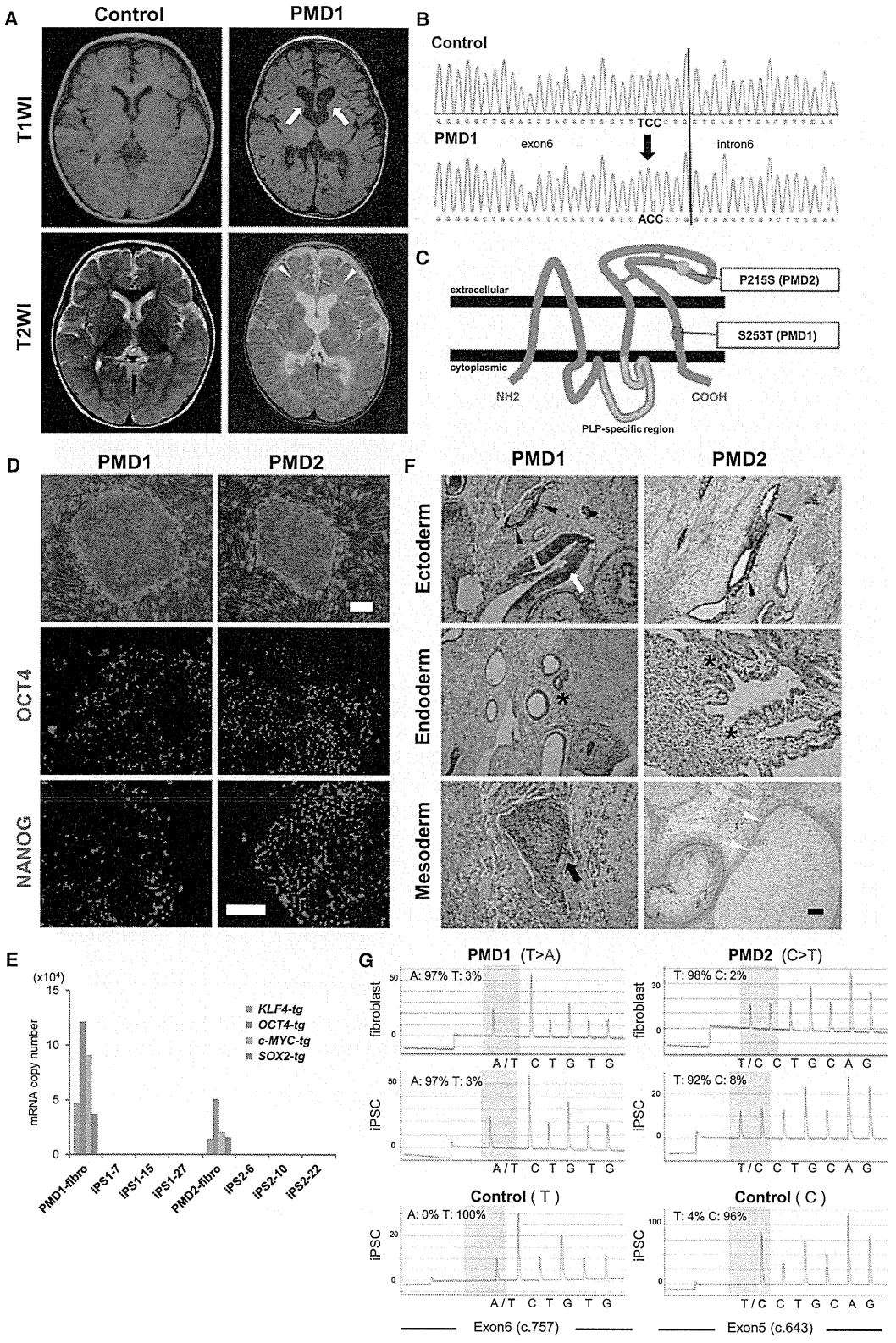

(legend on next page)

Both Control and PMD iPSCs Induce Oligodendrocyte Lineage Cells In Vitro

Based on the previously reported methods for inducing OLs from human ESCs and iPSCs (Hu et al., 2009; Izrael et al., 2007; Kang et al., 2007), we established our own culture protocol to induce OLs by modifying previously established protocols for efficiently differentiating human ESCs and iPSCs into neural stem/progenitor cells (NS/PCs) as neurospheres through EB formation (Nori et al., 2011; Okada et al., 2008). First, dorsomorphin (a bone morphogenetic protein signal inhibitor), SB431542 (a transforming growth factor β [TGF-β] receptor inhibitor), and BIO (a GSK3 inhibitor) were added during the early phase of EB formation to facilitate differentiation into NS/PCs more efficiently. Quantitative RT-PCR analysis of the expression of the NS/PC marker *SOX1* in EBs revealed a significantly higher induction efficiency of NS/PCs in our protocol with DSB (DSB: dorsomorphin, SB431542, and BIO) compared with those in our previously established methods (control, DSB−) or those in the previously reported dual Smad inhibition with DS (Figure 2B). We also added retinoic acid for caudalization and purmorphamine (Sonic hedgehog agonist) for ventralization during EB formation until EB dissociation. Then, the dissociated EBs were cultured in suspension to form neurospheres in proliferation medium supplemented with factors that promote the commitment and proliferation of OL lineage cells (Shimada et al., 2012). For adherent differentiation, neurospheres were cultured in differentiation medium supplemented with factors that promote the commitment of OL lineage cells as indicated in the Experimental Procedures (Figure 2A). From the quantitative RT-PCR analysis in this protocol, the pluripotent marker (*NANOG*) was notably downregulated in the EB stage, and other lineage markers (mesodermal and endodermal markers, such as *BRACHYURY* and *SOX17*) were not detected in any stage. The NS/PC marker (*SOX1*) was upregulated in the EB and neurosphere stages and gradually downregulated after adherent differentiation (differentiation stage; Figure 2C). The expression profiles were similar between the control, PMD1, and PMD2 iPSCs (Figure S1A available online). To reveal the differentiation potentials of neurospheres, we performed immunocytochemistry of differentiated neurospheres for markers of neurons (βIII tubulin), astrocytes (GFAP), and oligodendrocytes (O4; Figures 2E and 2F) and a time course analysis of the expression levels of neuronal and glial markers through quantitative RT-PCR (Figure 2D). The expression profiles were similar between the control and PMD1 and PMD2 cells (Figure S1B). Based on these analyses, we confirmed the differentiation potentials of the iPSCs into three neural lineage cells and the reproducibility of our differentiation protocol. Regarding the differentiation potentials of OL lineage cells, all PMD-iPSCs and control iPSCs were able to induce platelet-derived growth factor receptor α (PDGFRα)$^+$-OL progenitor cells (OPCs), O4$^+$-immature OLs (immature OLs), and myelin basic protein (MBP)$^+$-mature OLs (mature OLs) with typical morphologies (Figure 3B). OPCs were also positive for NG2 (Figure 3A). In contrast, myelin protein zero (MPZ)-positive cells, a major structural protein of peripheral myelin, could not be detected, indicating that these cells were oligodendrocytes, but not schwann cells.

After 55–70 days in vitro (DIV), OPCs were observed in 86.3% of the colonies of control cells and 95.1% and 90.5% of the colonies of PMD1 and PMD2 cells, respectively. At 70–85 DIV, immature OLs were observed in 77.8% of control colonies and 93.8% and 93.8% of the colonies of PMD1 and PMD2 cells, respectively. At 80–95 DIV, mature OLs were observed in 74.9% of the colonies of control cells and 93.8% and 89.2% of the colonies of PMD1 and PMD2 cells, respectively (Figure 3C). No significant

Figure 1. Features of the PMD Patients and Characterization of iPSCs

(A) MRI images of the brains of patient PMD1 (right) and an age-matched control (left). Mild and diffuse atrophy of the brain, dilatation of the ventricles (open arrow), and diffuse high-intensity signals in the white matter (open arrowhead) are shown. T1WI, T1-weighted images; T2WI, T2-weighted images.

(B) Direct sequencing analysis of genomic DNA from PMD1's leukocytes showed a missense mutation c.757 T > A (p.Ser253Thr) in exon 6 of the *PLP1* gene.

(C) Schematic representation of the mutation sites in PMD1 and PMD2.

(D) Representative morphology of iPSC colonies (above) and immunochemical analysis of pluripotent markers, NANOG and OCT4 (below). The scale bars represent 200 μm.

(E) Quantitative RT-PCR analysis of the expression of retroviral transgenes in established PMD iPSC clones. Data are presented as the mRNA copy numbers for each transgene divided by those for *β-actin*.

(F) Representative H&E staining of teratomas derived from established PMD iPSC clones. Teratomas were formed via the injection of undifferentiated iPSCs into the testes of NOD/SCID mice. Open arrow, neural rosettes. Arrowhead, pigmented epitheliums. Asterisks, goblet cells. Arrow, bones. Open arrowhead, cartilage. The scale bars represent 200 μm.

(G) Representative pyrosequencing analysis of the mutations in the *PLP1* gene in fibroblasts and iPSCs. Identical mutations to those observed in the patients' fibroblasts (PMD1, 757 T > A; PMD2, 643 C > T) were confirmed in all the iPSC clones.

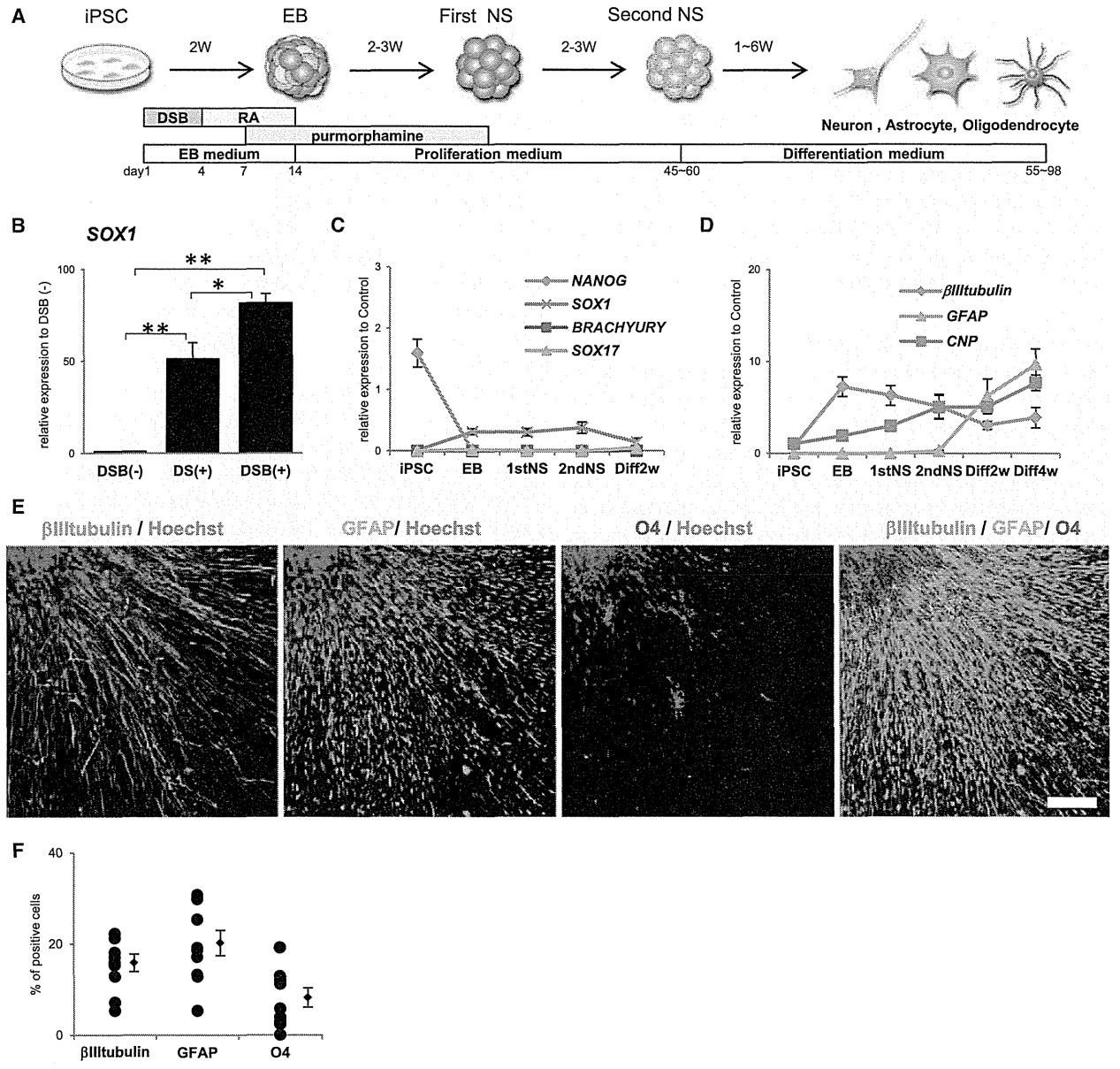

Figure 2. Differentiation Potential of Human iPSCs

(A) Schematic presentation of the protocols for OL differentiation from hiPSCs. DSB, dorsomorphine (D), SB431542 (S), and BIO (B); RA, retinoic acid; NS, neurospheres.

(B) Quantitative RT-PCR analysis of *SOX1* expression in EBs, suggesting a significantly higher induction efficiency of NS/PCs in EBs in our protocol with DSB (DSB: dorsomorphin, SB431542, and BIO) compared with those in our previously established methods (control, DSB−) or those in the previously reported method with dual Smad inhibition (DS) (n = 3, mean ± SEM; independent experiments; $*p < 0.05$; $**p < 0.01$; t test).

(C) Quantitative RT-PCR analysis of the expression of cell-type-specific markers at each differentiation stage. *NANOG* (a pluripotent marker) was readily downregulated in the EB stage. Other lineage markers (mesodermal and endodermal markers, such as *BRACHYURY* and *SOX17*) were not detected in any stage. *SOX1* was upregulated in EB and neurosphere stage in control iPSC clones (201B7, WD39, and TIG121; n = 3; mean ± SEM; independent experiments).

(D) Quantitative RT-PCR analysis of differentiated neurospheres for the markers of neurons (*βIII tubulin*), astrocytes (*GFAP*), and oligodendrocytes (*CNP*) in control iPSC clones (201B7, WD39, and TIG121; n = 3; mean ± SEM; independent experiments).

(legend continued on next page)

differences were detected in either control or PMD with regard to OL lineage differentiation efficiency.

To examine the proportion of immature and mature OL lineage cells, we performed immunocytochemistry for OLIG2, PDGFRα, and MBP after 2 or 4 weeks differentiation of control-iPSC-derived second neurospheres containing more than 40 OLIG2-positive cells and counted the number of marker-positive cells (Figures 3D and 3E). After 2 and 4 weeks of differentiation, OLIG2$^+$ and PDGFRα$^+$ OPCs were abundantly observed. After 4 weeks of differentiation, small numbers of MBP$^+$ mature OLs appeared.

Involvement of ER Stress in PMD

Previous in vitro transfection studies in nonglial cells have indicated that various PLP1 mutants accumulate in the ER immediately after translation, in contrast to the distribution of wild-type PLP1 at the plasma membrane (Gow et al., 1994; Gow and Lazzarini, 1996; Thomson et al., 1997). Therefore, we next examined the expression of PLP1 proteins via immunocytochemistry. When stained with anti-PLP1 and MBP antibodies, the membrane protein PLP1 was observed to be dispersed into the processes of OLs and to colocalize with MBP in control iPSC-derived mature OLs. However, in PMD1 and PMD2 iPSC-derived mature OLs, PLP1 protein staining was not observed in the OL processes; instead, PLP1 protein staining localized to the perinuclear cytoplasm (Figure 4A). Thus, we also performed staining for the ER marker KDEL and found that the mislocalized PLP1 proteins colocalized with KDEL (Figures 4A and 4B). All of the control iPSC-derived OLs showed staining for PLP1 proteins in the processes of mature OLs, whereas all of the PMD iPSC-derived mature OLs only exhibited PLP1 protein localization in the ER. These results suggest that mutant PLP1 proteins accumulated in the ER and triggered ER stress in mature OLs derived from PMD-iPSCs.

We next examined the expression of ER stress markers in OLs. O4$^+$ cells were isolated from both the PMD and control iPSC-derived differentiated cells 4 weeks after the attachment of the second neurospheres via magnetic-activated cell sorting (MACS) using an anti-O4 antibody. The purified O4$^+$ cells underwent quantitative RT-PCR to determine the expression of ER stress markers (*BIP*, *CHOP*, and spliced *XBP1*). No significant differences were detected between the control and PMD iPSC-derived OLs regarding the expression of ER stress markers under default conditions (Figure 4C). Therefore, we next examined the susceptibility of the iPSC-derived OLs to the extrinsic ER stress induced by treatment with a low concentration of tunicamycin 50 nM for 6 hr (known as an ER-stress inducer). The results showed that the expression of all ER-stress markers was significantly increased in tunicamycin-treated O4$^+$ cells relative to untreated O4$^+$ cells in PMD1 (Figure 4D). This result suggested that a higher susceptibility to ER stress was observed in PMD1 iPSC-derived OLs than in those derived from control and PMD2 iPSCs.

We next treated the iPSC-derived OLs with a higher concentration of tunicamycin 100 nM for 6 hr and examined the expression levels of ER stress markers. PMD2 iPSC-derived OLs showed significantly higher expression levels of spliced *XBP1*, the most sensitive ER stress marker, than control iPSC-derived OLs (Figure 4E). No significant differences were detected in the expression levels of *BIP* and *CHOP* between control and PMD2. Taken together, these results suggest that ER stress is involved in the pathogenesis of the PMD patients with PLP1 missense mutations, and a higher susceptibility to ER stress was observed in PMD1 iPSC-derived OLs than in those derived from PMD2, which is consistent with the more severe phenotypes of the PMD1 patient compared with the PMD2 patient.

Increased Apoptosis Is Observed in PMD iPSC-Derived Oligodendrocytes

In addition to their susceptibility to ER stress, the PMD iPSC-derived OLs showed significant morphological differences, as revealed by O4 staining, such as scattered O4 staining in their processes compared with control iPSC-derived OLs, which exhibited uniform O4 staining in their processes (Figure 5A). Thus, to investigate the apoptotic processes of PMD iPSC-derived OL lineage cells, we examined the expression of cleaved caspase-3 (apoptotic marker) in O4$^+$-immature OLs and MBP$^+$-mature OLs via immunostaining. Some of the PMD iPSC-derived OLs that showed scattered O4 staining in their processes were positive for cleaved caspase-3 (Figure 5B). The numbers of cleaved caspase-3$^+$ cells in both PMD1 and PMD2 iPSC-derived immature OLs and mature OLs were significantly increased compared with those derived from control iPSCs (Figure 5C). We next performed immunocytochemistry for KI67 and OLIG2. We found that the proportion of OLIG2$^+$ cells and KI67$^+$ cells among OLIG2$^+$ cells were unchanged between PMD and control samples, suggesting that the compensatory proliferation of OPCs for increased apoptosis in PMD iPSC-derived OLs is unlikely (Figures S2A and S2B). Therefore, although

(E) Representative low-magnification images of the immunocytochemistry of three neural lineage cells (neurons: βIII tubulin; astrocytes: GFAP; oligodendrocytes: O4). The scale bar represents 100 μm.
(F) Quantitative analysis of the percentages of three neural lineage cells in control-iPSCs (201B7, WD39, and TIG121)-derived neurospheres (n = 9; mean ± SEM; independent experiments).

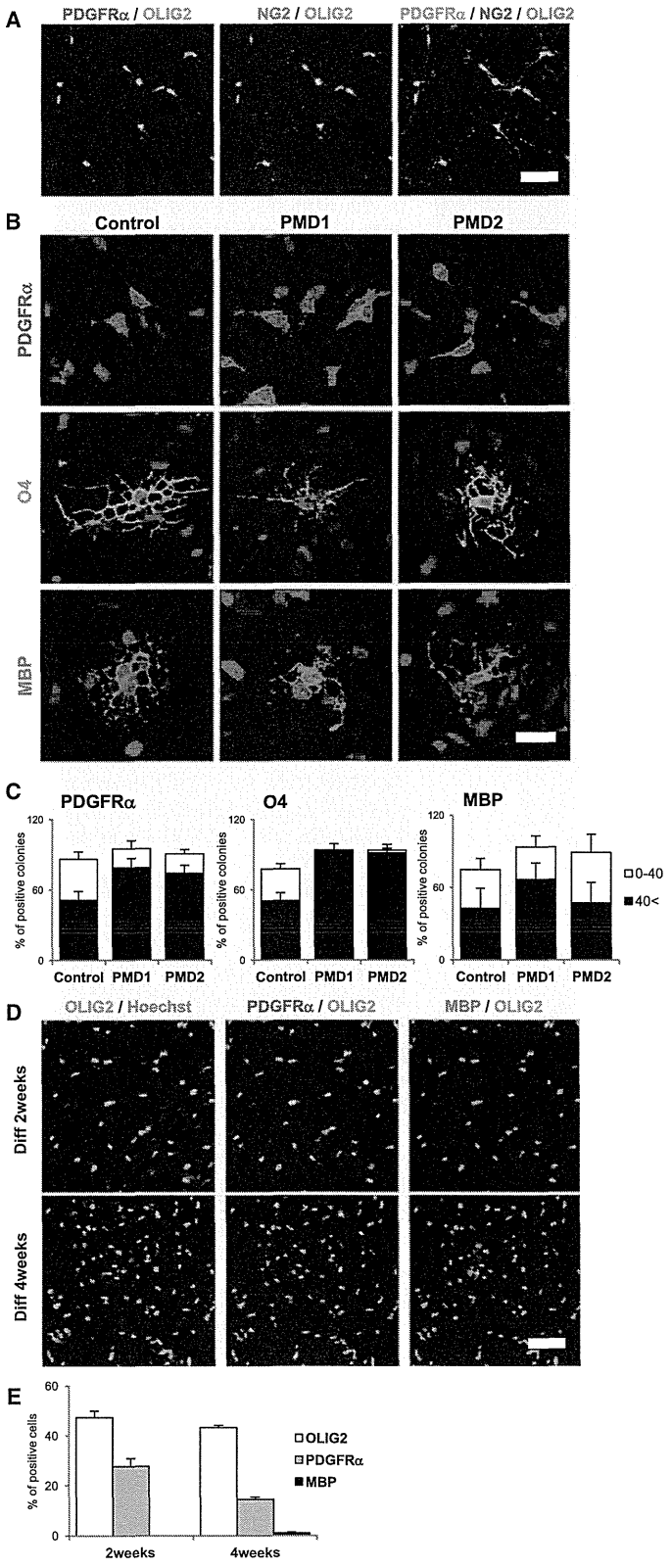

Figure 3. Differentiation Potential of Human iPSCs into Oligodendrocytes

(A) Representative image of immunocytochemistry for OPC markers (PDGFRα and NG2). OPCs were positive for both PDGFRα and NG2. The scale bar represents 50 μm.

(B) Representative image of immunocytochemistry of differentiated neurospheres using markers for OL lineage cells. Both control and PMD iPSCs differentiated into PDGFRα$^+$-OL progenitor cells (OPCs), O4$^+$-immature OLs (immature OLs), and MBP$^+$-mature OLs (mature OLs). The scale bar represents 20 μm.

(C) Quantitative analysis of the differentiation efficiency into OL lineage cells. The numbers of neurosphere colonies containing more than 40 marker-positive cells (≥40 cells; oligodendrocyte [++]), those containing less than 40 marker-positive cells (1–39 cells oligodendrocyte [+]), and those without marker-positive cells (oligodendrocyte [−]) were counted and are presented as the percentage of total neurosphere colonies. Oligodendrocyte (++) neurosphere colonies and oligodendrocyte (+) neurosphere colonies are indicated by black and white bars, respectively (PDGFRα, n = 6; O4, n = 6; MBP, n = 4; mean ± SEM; independent experiments). No significant difference was detected among control (201B7, WD39, and TIG121) and PMD iPSCs (PMD1-7, PMD1-15, and PMD1-27 and PMD2-6, PMD2-10, and PMD2-22)-derived OL lineage cells ($p > 0.05$; Mann-Whitney's U test).

(D) Representative image of immunocytochemistry for OLIG2, PDGFRα, and MBP after 2 or 4 weeks differentiation of control-iPSC-derived second neurospheres containing more than 40 OLIG2-positive cells. The scale bar represents 50 μm.

(E) Quantitative data of the percentages of PDGFRα$^+$ cells/OLIG2$^+$ cells and MBP$^+$ cells/OLIG2$^+$ cells (after 2 or 4 weeks of differentiation) in control-iPSC (201B7, WD39, and TIG121)-derived neurospheres containing more than 40 OLIG2-positive cells. (n = 3; mean ± SEM; independent experiments). After 2 and 4 weeks of differentiation, OLIG2$^+$ and PDGFRα$^+$ OPCs were abundantly observed. After 4 weeks of differentiation, small numbers of MBP$^+$ mature OLs appeared.

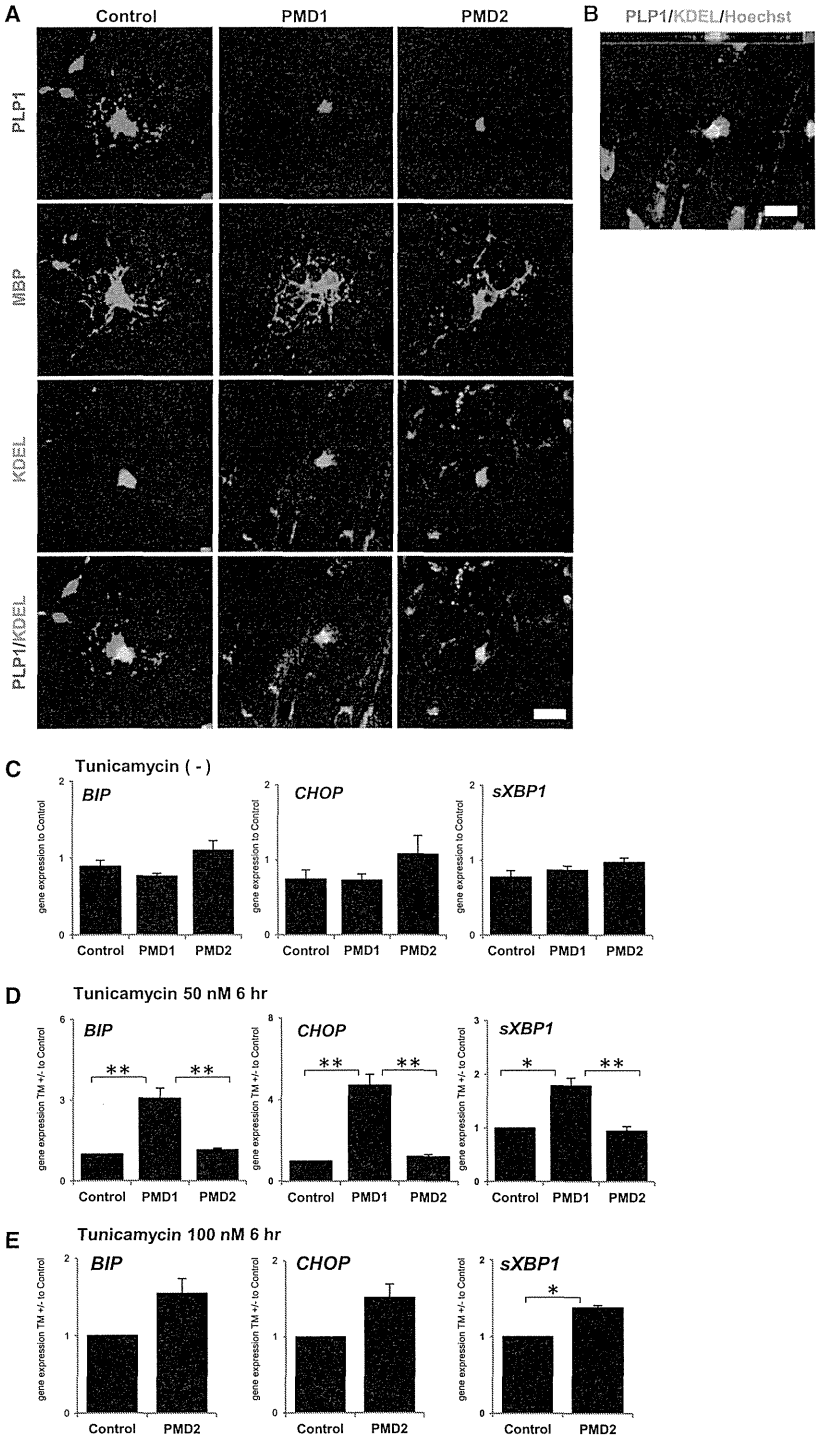

Figure 4. Involvement of ER Stress in PMD-Derived Oligodendrocytes

(A) Representative immunocytochemistry image for PLP1, the OL marker MBP, and the ER marker KDEL. In the control iPSC-derived mature OLs, the PLP1 protein localized to both the ER (KDEL) and membrane, whereas in the PMD iPSC-derived OLs, the mutant PLP1 protein only localized to the ER. The scale bar represents 20 μm.

(B) Three-dimensional image of mature OLs derived from PMD1 iPSCs showing colocalization of the mutant PLP1 protein and KDEL via confocal laser scanning microscopy. The scale bars represent 20 μm.

(C) Quantitative RT-PCR analyses of the expression of ER stress markers in $O4^+$ cells. The data are presented as the expression relative to that in iPSCs. No significant differences were observed between the control iPSC (201B7, WD39, and TIG121) and PMD iPSC (PMD1-7, PMD1-15, and PMD1-27 and PMD2-6, PMD2-10, and PMD2-22)-derived cells (n = 5; mean ± SEM; independent experiments; t test).

(D) Quantitative RT-PCR analyses of the expression of ER stress markers in tunicamycin-treated (50 nM; 6 hr) $O4^+$ cells relative to untreated $O4^+$ cells. A higher level of stress susceptibility was detected in PMD1 (PMD1-7, PMD1-15, and PMD1-27) than in control (201B7, WD39, and TIG121) and PMD2 (PMD2-6, PMD2-10, and PMD2-22; n = 5; mean ± SEM; independent experiments; *p < 0.05; **p < 0.01; Mann-Whitney's U test).

(E) Quantitative RT-PCR analyses of the expression of ER stress markers in tunicamycin-treated (100 nM; 6 hr) $O4^+$ cells relative to untreated $O4^+$ cells. PMD2 iPSC (PMD2-6, PMD2-10, and PMD2-22)-derived OLs showed significantly higher expression levels of spliced *XBP1* than control iPSC (201B7, WD39, and TIG121)-derived OLs (n = 3; mean ± SEM; independent experiments; *p < 0.05; t test).

the differentiation efficiency into oligodendrocyte lineage cells was unchanged between PMD and control (Figure 3C), considering that anti-O4 and anti-MBP antibodies stain both apoptotic and live OLs (Figures 5A and 5C), the increased levels of apoptosis resulted in decreased numbers of live OLs in PMD iPSC-derived cultures.

Because previous reports have indicated the neurotrophic actions of PLP1 (Griffiths et al., 1998; Yin et al.,

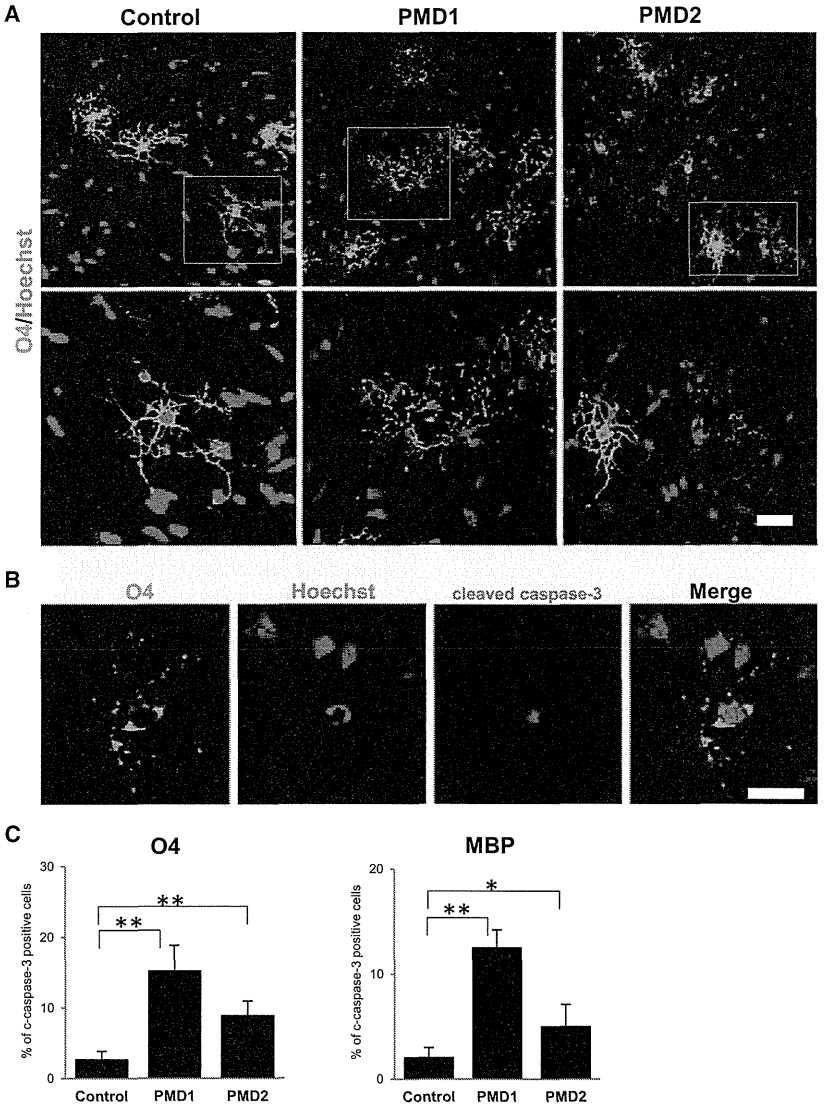

Figure 5. Enhanced Apoptosis in PMD iPSC-Derived Oligodendrocytes

(A) Morphological differences in OLs. Immunocytochemical analysis of iPSC-derived OLs for OLs marker (O4) and nuclei (Hoechst). The OLs showed a uniform appearance in the control iPSC-derived cells but showed scattered morphologies in the PMD iPSC-derived cells. The scale bar represents 40 μm.

(B) Representative immunocytochemical images of apoptotic OLs using markers for apoptosis (cleaved caspase-3) and OLs (O4). OLs ($O4^+$ or MBP^+) that were both positive for cleaved caspase-3 and showed nuclear condensation or fragmentation were considered apoptotic OLs. The scale bar represents 40 μm. c-caspase-3, cleaved caspase-3.

(C) Quantitative analysis of the number of apoptotic OLs. The number of apoptotic cells was higher in the PMD1 (PMD1-7, PMD1-15, and PMD1-27) and PMD2 iPSC (PMD2-6, PMD2-10, and PMD2-22)-derived OLs than control iPSC (201B7, WD39, and TIG121)-derived OLs ($n = 9$; mean ± SEM; independent experiments; $^*p < 0.05$; $^{**}p < 0.01$; Mann-Whitney's U test).

2006), we next investigated whether apoptosis was induced in PMD patient-derived neurons. However, no cleaved caspase-3^+ neurons derived from either control or PMD iPSCs were observed (Figure S2C), suggesting that this increased apoptosis was specific to oligodendrocyte lineage cells in PMD in our iPSC-derived cultures.

Abnormal Myelin Structures and ER Morphologies Were Detected by Electron Microscopic Analysis

Finally, we focused on the myelinating properties of PMD iPSC-derived OLs, which represent the most characteristic pathogenic feature of PMD. Because different types of neural cells, including neurons and astrocytes, in addition to OLs, were derived in our cultures, neuron-glial interactions could be observed and neuron myelination by the iPSC-derived OLs could be analyzed in situ. In immunocytochemical analysis of MBP and NF200 (neurofilament marker), parts of the neurofilament$^+$ neurites were wrapped by the MBP^+ process of iPSC-derived oligodendrocytes (Figure S3A). Thus, to evaluate the histological abnormality of the myelin structures in vitro, we performed transmission electron microscopy (TEM) analysis of ultrathin sections of the differentiated cells. The results showed that myelin structures with or without axons could be observed via TEM. Considering the neuronal processes wrapped by the MBP^+ process of iPSC-derived OLs observed through immunocytochemistry, some of the axonal structures could have been lost during the fixation process for TEM.

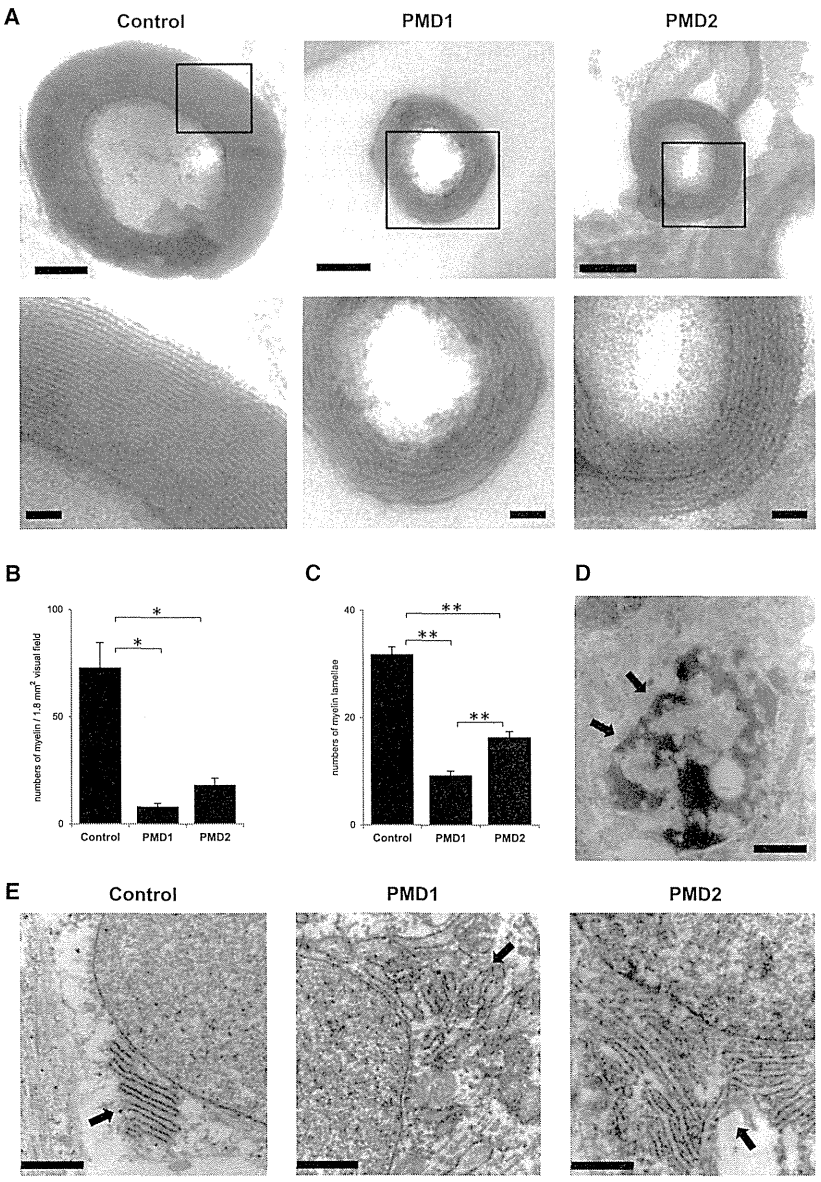

Figure 6. Electron Microscopic Analysis of PMD iPSC-Derived Cells

(A) TEM of iPSC-derived cells. The maximum number of normal myelin lamella was greater than 30 in the control iPSC-derived myelin sheaths. In contrast, a limited number of myelin lamella was observed in the PMD iPSC-derived myelin sheaths. High-magnification images are also shown in the lower panel. The scale bars represent 100 nm (upper panels) and 20 nm (lower panels).

(B) Quantitative analysis of the numbers of myelin structures. We counted the numbers of myelin structures per visual field of EM images (approximately 1.8 mm^2) for the myelination frequency. The frequency of myelin formation was significantly decreased in both PMD1 (PMD1-7, PMD1-15, and PMD1-27) and PMD2 (PMD2-6, PMD2-10, and PMD2-22) iPSC-derived OLs (n = 3; mean ± SEM; independent experiments; *p < 0.05; t test).

(C) Quantitative analysis of the numbers of myelin lamellae. We counted the numbers of major dense lines per myelinated fiber for the thickness of myelin, and the average of the numbers of myelin lamellae in the top ten myelin sheaths are presented. The thickness of the myelin sheath was greatly reduced in both PMD1 (PMD1-7, PMD1-15, and PMD1-27) and PMD2 (PMD2-6, PMD2-10, and PMD2-22) iPSC-derived OLs (n = 3; mean ± SEM; independent experiments; **p < 0.01; t test).

(D and E) Histological abnormalities detected in PMD iPSC-derived cells via TEM. Apoptotic cells with fragmented nuclei (arrow in D) were frequently detected among the PMD-iPSC-derived cells (D). The scale bar represents 1 μm. Dilations of ER intermembrane spaces were also observed (E). The scale bars represent 0.5 μm.

Although we stained with antibodies against NAV1.6 (nodes) and CASPER (paranodes), we could not detect any significant staining in our cultures. This may suggest immature myelination in the present culture conditions.

Notably, mature myelin structures with thick myelin lamella ~30 layers were observed in the control cultures. In contrast, in the PMD iPSC-derived cultures, a limited number of myelin structures with thin myelin lamella ~15 layers were observed (Figure 6A). The frequency of myelin formation and thickness of the myelin sheath were significantly decreased in both PMD1 and PMD2 iPSC-derived OLs (Figures 6B and 6C).

In addition, several types of histological abnormalities were detected in the PMD cells. Apoptotic cells exhibiting nuclear condensation were frequently observed among the PMD iPSC-derived cells, in contrast to that observed in those derived from control iPSCs (Figure 6D). Moreover, aberrant ER morphologies, such as dilation of the ER intermembrane space (Fan et al., 2013; Lim et al., 2011), were found in the PMD iPSC-derived cells (Figure 6E). These results indicate that PMD iPSC-derived OLs develop a poor myelin structure and subsequently die, supporting the involvement of ER stress in the pathogenesis of PMD.

DISCUSSION

In this study, we established PMD-specific human iPSCs from two patients with different clinical severity and different missense mutations of *PLP1*. One mutation is in the transmembrane domain (PMD1) and the other is in the extracellular domain (PMD2), both of which differ from those in the previously reported PMD animal models. And we generated patient-specific OLs. This model enables an investigation of the correlations between the molecular pathophysiology of PMD and various cell biological phenomena, including OL differentiation, myelination, and apoptosis in patient-derived live OLs through morphological, biochemical, and molecular biological methods. These analyses could not be achieved using conventional disease models.

Although there are several reported methods for inducing OPCs from human ESCs (Hu et al., 2009; Izrael et al., 2007; Kang et al., 2007), these methods have difficulties in reproducibility, making it difficult to obtain sufficient amounts of mature OLs for analysis. In the present study, we developed an improved neural differentiation protocol for human pluripotent stem cells by utilizing an EB-neurosphere method involving dual Smad inhibition in combination with a GSK3 inhibitor to facilitate differentiation into NS/PCs more efficiently and reproducibly. In addition, the use of T3, ciliary neurotrophic factor (CNTF), and leukemia inhibitory factor (LIF) was beneficial for differentiation into OLs. Using this method, we achieved stable differentiation of several human iPSC clones into OLs in a similar manner to that reported in a recent study (Wang et al., 2013). Remarkably, our culture procedure enabled recapitulation of myelin formation in human iPSC (hiPSC)-derived neurites and OLs in vitro in a single-culture system without coculturing with other cells, such as rodent hippocampal neurons, as previously reported (Kang et al., 2007). Thus, this study reports a successful in vitro myelination assay using human iPSC-derived neurons and OLs.

Another important finding of this study was that the differentiation of PMD iPSCs into OLs well-recapitulated the progression of PMD pathogenesis in vitro. Although the PMD-specific iPSCs induced abundant MBP^+ mature OLs, myelination was substantially less frequent and limited lamella formation was observed. These results suggest that incomplete maturation and limited survival of OLs rather than a failure to differentiate into OLs is responsible for PMD pathogenesis. However, the cause of OL degeneration and dysmyelination observed in PMD is unclear. Some previous reports have demonstrated the involvement of ER stress in the pathogenesis of PMD associated with missense mutations in the *PLP1* gene. Analyses using cell lines, such as cos7 cells transfected with wild-type or mutant *PLP1* genes, have shown that wild-type PLP1 protein is synthesized in the ER and transported to the cell surface, whereas mutant PLP1 proteins are arrested in the secretory pathway at an early stage and accumulate in the ER (Gow et al., 1994). In the CNS of PMD model mice, such as msd and rsh mice, mutant PLP1 proteins are largely confined to the perinuclear region of OLs and involved in the UPR (Gow et al., 1998). These reports suggest the involvement of ER stress in PMD pathogenesis. In the present study, accumulation of misfolded mutant PLP1 proteins in the ER and high susceptibility to ER stresses in the PMD1 and PMD2 cells were observed. This increased susceptibility to ER stresses or other cellular response could have resulted in the apoptosis of PMD iPSC-derived OLs and immature/incomplete myelination.

In addition, we detected differences between PMD1 and PMD2 cells. The differences of susceptibility to ER stresses and the thickness of the myelin sheath were consistent with the different levels of clinical severity of the two patients. The correlations between different clinical severity, different missense mutations, and different pathogenic changes have not previously been reported by conventional disease models. These results suggest that this PMD model accurately recapitulates disease pathophysiology not only qualitatively but also in terms of the degree of disease progression, although how the different point mutations affect the degree of the observed phenotype must be clarified. Accordingly, we propose models for a "proof-of-concept" of PMD pathogenesis based on the endogenous mutations found in PMD iPSC-derived OLs. The present findings cannot be generalized to PMD as a whole because the more common *PLP1* duplication was not included; therefore, we will investigate the pathogenesis of PMD with *PLP1* duplications in the future.

The current study represents the a demonstration of pathogenic changes in PMD patients with *PLP1* missense mutations using disease-specific, human iPSC-derived OLs. This model faithfully reproduces the pathophysiology observed in the CNS of PMD patients, which is difficult to identify through conventional experiments. Moreover, our results demonstrate the usefulness of iPSC-derived OLs for the analysis of the pathogenic processes of dysmyelinating human neurological disorders and the development of novel therapeutic agents for their treatment.

EXPERIMENTAL PROCEDURES

Isolation of Human Skin Fibroblasts and Generation of iPSCs

HDFs from the dermis of a 1-year-old Japanese male patient and HDFs from the dermis of a 20-year-old Caucasian male patient (Coriell Institute: GM09546) were used to establish PMD1-iPSCs (PMD1-7, 1-15, and 1-27) and PMD2-iPSCs (PMD2-6, 2-10, and

2-22), respectively. Additional control cell lines used in this study included 201B7 (control A, established from HDFs [Cell Applications] from the dermis of a 36-year-old Caucasian female; Takahashi et al., 2007), WD39 (control B, established from HDFs from the dermis of a 16-year-old Japanese female; Imaizumi et al., 2012), and TIG121 (control C, established from HDFs from the dermis of an 8-month-old Japanese male [Japan Health Sciences Foundation]). All of the human iPSC clones were established through the retroviral transduction of four transcription factors (*SOX2*, *OCT4*, *KLF4*, and *c-MYC*) into HDFs as described previously (Takahashi et al., 2007) and evaluated based on the expression of pluripotent markers, the silencing of retroviral transgenes, and teratoma formation assays as described previously (Ohta et al., 2011). We used three clones for each group for further analysis: control (201B7, WD39, and TIG121), PMD1 (1-7, 1-15, and 1-27), and PMD2 (2-6, 2-10, and 2-22). The data from the three clones were combined in each figure, and the data are shown as the average of the three clones. All of the experimental procedures for iPSC production were approved by the ethics committee of the Keio University School of Medicine (approval number: 20-16-18).

Culture and In Vitro Differentiation of Human iPSCs

hiPSCs were grown on mitomycin-C-treated SNL murine fibroblast feeder cells in gelatin-coated (0.1%) tissue culture dishes. The hiPSCs were maintained in standard hESC medium (Dulbecco's modified Eagle's medium [DMEM]/F12 [Sigma] containing 20% KnockOut serum replacement [KSR; Life Technologies], nonessential amino acids [NEAA], 0.1 mM 2-mercaptoethanol [Sigma], and 4 ng/ml fibroblast growth factor 2 [FGF-2] [PeproTech]) at 37°C in a humidified atmosphere of 3% CO_2.

For in vitro differentiation, iPSC colonies were detached from the feeder layers en bloc using a dissociation solution (0.25% trypsin, 100 μg/ml collagenase IV [Invitrogen], 1 mM $CaCl_2$, and 20% KSR; day 0) and cultured in suspension in bacteriological dishes to form EBs in a humidified atmosphere of 3% CO_2. From day 1 to 4 of EB formation, 3 μM dorsomorphin (Sigma), 3 μM SB431542 (Tocris Bioscience), and 3 μM BIO ((2′Z, 3′E)-6-bromoindirubin-3′-oxime; Sigma) were added. In addition, 1 μM retinoic acid (Sigma) and 1 μM purmorphamine (Calbiochem) were added on days 4 and 7, respectively, and maintained thereafter until day 16 (EB dissociation). The medium was changed every 2 days. On day 16, the EBs were enzymatically dissociated into single cells using TrypLE Select (Life Technologies), and the dissociated cells were cultured in suspension at a density of 1×10^5 cells/ml in proliferation medium consisting of serum-free medium (media hormone mix [MHM]; Okada et al., 2008) supplemented with 2% B27 supplement (Invitrogen), NEAA, 1 μM purmorphamine, 60 ng/ml T3 (Sigma), 10 ng/ml PDGF-AA (PeproTech), 20 ng/ml FGF, 10 ng/ml epidermal growth factor (PeproTech), 10 ng/ml insulin growth factor 1, and 10 ng/ml neurotrophin-3 (R&D Systems) in a humidified atmosphere of 5% CO_2. The medium was changed every 4~6 days for approximately 15~20 days to form the first neurospheres. To passage neurospheres, the first neurospheres were dissociated in the same manner as described above and cultured at a density of 1×10^5 cells/ml in proliferation medium without purmorphamine for approximately 15~20 days. To assay neurosphere differentiation, undissociated 5–7 neurospheres were plated onto coverslips 10 mm in diameter coated with poly-L-ornithine (Sigma) and growth-factor-reduced Matrigel (50× dilution, thin coated; Invitrogen), and cultured in differentiation medium that consisted of MHM supplemented with 2% B27 supplement, NEAA, 60 ng/ml T3, 10 ng/ml hLIF (Millipore), and 25 ng/ml CNTF (R&D Systems) for 2–6 weeks in a humidified atmosphere of 5% CO_2. Half of the medium was changed every 2 or 3 days. For the quantitative analysis of the differentiation efficiency into OL lineage cells, the numbers of neurosphere colonies containing more than 40 marker-positive cells (≥40 cells, oligodendrocyte [++]), those containing less than 40 marker-positive cells (1–39 cells, oligodendrocyte [+]), and those without marker-positive cells (oligodendrocyte [−]) were counted and are presented as the percentage of total neurosphere colonies. To examine the expression of ER-stress markers, $O4^+$ differentiated cells were purified 4 weeks after the attachment of the neurospheres using MACS technology with an anti-O4 antibody.

Direct Sequencing and Pyrosequencing Analysis of the *PLP1* Gene

Genomic DNA was extracted from peripheral blood samples (leukocytes) from PMD1 and from HDFs and iPSCs from both PMD1 and PMD2. For direct sequencing of the mutations in the *PLP1* gene in PMD1, fragments of the promoter regions (5′ UTR) and all seven exons of the *PLP1* gene were amplified via PCR. The PCR primers and cycling conditions employed for direct sequencing are listed in Table S1. For pyrosequencing analysis of the mutations in the *PLP1* gene in HDFs and iPSCs, fragments containing the PMD1 mutation (c.757 T > A in exon 6) and PMD2 mutation (c.643 C > T in exon 5) were amplified via PCR using forward primers and biotinylated reverse primers. Pyrosequencing analyses were performed following the manufacturer's instructions (Pyromark Q24; QIAGEN). The PCR primers and cycling conditions applied for pyrosequencing analysis are listed in Table S2.

RNA Isolation and RT-PCR

RNA isolation and real-time quantitative RT-PCR were performed as previously described using SYBR Premix ExTaq II and the MX3000P Real-Time PCR system (Stratagene; Okada et al., 2004, 2008). The amount of cDNA was normalized to that of human-specific *β-ACTIN* mRNA.

For the analysis of the expression of retroviral transgene in iPSCs, HDFs 7 days after the retroviral introduction (day 11 of the protocol) of four genes (*SOX2*, *OCT4*, *KLF4*, and *c-MYC*) were used as the positive control (*SOX2* tg, *OCT4* tg, *KLF4* tg, and *c-MYC* tg). The data are presented as the copy numbers of mRNA for each transgene. As for the analyses of *NANOG*, *SOX1*, *BRACHYURY*, *SOX17*, *βIII tubulin*, *GFAP*, *CNP*, and ER stress marker (*BIP*, *CHOP*, and *spliced XBP1*), data are presented as the relative expression to that in control. The applied primer sequences and PCR cycling conditions are listed in Table S3.

Immunocytochemical Analysis

For immunocytochemical analysis, cells were fixed with 4% paraformaldehyde for 30 min at room temperature. After blocking in

blocking buffer (PBS containing 10% normal goat or donkey serum and 0.3% Triton X-100) for 1 hr at room temperature, the cells were incubated with primary antibodies at 4°C overnight. For O4 staining, we used blocking buffer without Triton X-100. After three washes with PBS, the cells were incubated with Alexa 488-, Alexa 555-, or Alexa 647-conjugated secondary antibodies (Life Technologies) for 1 hr at RT. Nuclei were stained with 10 μg/ml Hoechst 33258 (Sigma). After washing with PBS, the cells were mounted on slides and examined with a universal fluorescence microscope (Axiophoto; Carl Zeiss) or confocal laser scanning microscope (LSM700; Carl Zeiss). The primary antibodies used in these analyses were as follows: NANOG (1:100; ReproCELL), OCT4 (1:500; Santa Cruz Biotechnology), OLIG2 (1:1,000; R&D Systems), PDGFRα (1:2,000; Santa Cruz Biotechnology), NG2 (1:2,000; Millipore), O4 (1:5,000; Millipore), MBP (1:1,000; Serotec), β-III-tubulin (1:1,000; Sigma), NF200 (1:1,000, Millipore), GFAP (1:4,000, Dako), KDEL (Abcam), PLP1 (1:30,000; gifted from Masayuki Itoh [National Center of Neurology and Psychiatry] recognizes PLP1, but not DM20), KI67 (1:10,000, Abcam), and cleaved caspase 3 (1:1,000, Cell Signaling Technology).

Teratoma Assay

Undifferentiated iPSCs (5×10^5 cells) were injected into the testes of 8-week-old male nonobese diabetic (NOD)/severe combined immunodeficiency (SCID) mice (Charles River Laboratories) as described previously (Ohta et al., 2011). Eight weeks after injection, the resultant tumors were dissected and fixed with 4% paraformaldehyde. Paraffin-embedded tissue sections were produced, and hematoxylin and eosin (H&E) staining was performed. Images were obtained using a BZ-9000 microscope (Keyence).

Transmission Electron Microscopy

For TEM analysis, neurospheres and cells in dishes were fixed with 2.5% glutaraldehyde in 50 mM phosphate buffer (PB) overnight at 4°C. After washing twice in 0.1 M PB, these samples fixed with 1% osmium tetroxide for 90 min, dehydrated through ethanol, and embedded in Epon. The neurospheres were dissected and fixed on the stage, followed by the preparation of ultrathin sections with a thickness of 70 nm using an ultramicrotome (Leica Microsystems). The sections were subsequently stained with uranyl acetate and lead citrate for 10 and 12 min, respectively. Finally, the sections were observed under a transmission electron microscope (JEOL model 1230), and images were captured with Digital Micrograph 3.3 (Gatan). For the quantitative analysis of myelination, the number of myelin lamellae, which is the number of major dense lines per myelinated fibers, was counted to assess myelin thickness and the number of myelinated fibers per visual field of electron microscopy (EM) images (approximately 1.8 mm^2) was counted to assess myelination frequency.

SUPPLEMENTAL INFORMATION

Supplemental Information includes three figures and three tables and can be found with this article online at http://dx.doi.org/10.1016/j.stemcr.2014.03.007.

ACKNOWLEDGMENTS

We are grateful to Prof. F. Urano (Washington University School of Medicine) for valuable comments and analysis of ER stress, Prof. M. Amagai (Keio University) for skin biopsies, I. Kuki (Osaka City General Hospital) for providing patient medical information, M. Itoh (National Center of Neurology and Psychiatry) for providing PLP1 antibody, T. Nagai (Keio University) for assistance with the TEM analyses, N. Kuzumaki (Keio University) for technical assistance, and all of the members of H.O.'s laboratory for their encouragement and support. This work was supported by funding from the Project for the Realization of Regenerative Medicine and Support for Core Institutes for iPS Cell Research from the Ministry of Education, Culture; Support for the Core Institutes for iPS Cell Research from the Ministry of Education, Culture, Sports, Science and Technology of Japan (MEXT; to H.O.); and a Grant-in-Aid for the Global COE Program from MEXT to Keio University. This work was also supported by a Grant-in-Aid for Young Scientists (B) from MEXT, a Keio University Grant-in-Aid for the Encouragement of Young Medical Scientists to Y.K.-N. from the Kanrinmaru-Project at Keio University, a Grant-in-Aid for Young Scientists (A) and a Grant-in-Aid for Scientific Research on Innovative Areas (Foundation of Synapse Neurocircuit Pathology) from MEXT, and JST-CIRM Collaborative Research Program funding awarded to Y.O. H.O. is a scientific consultant for SanBio, Inc., Eisai, Co., Ltd., and Daiichi Sankyo, Co., Ltd. M.S. and A.N. are employed by Takeda Pharmaceutical Company Limited. S.Y. is a member without salary of the scientific advisory boards of iPierian, iPS Academia Japan, Megakaryon Corporation, and HEALIOS K. K. Japan.

Received: October 8, 2013
Revised: March 20, 2014
Accepted: March 20, 2014
Published: April 24, 2014

REFERENCES

Fan, J., Long, H., Li, Y., Liu, Y., Zhou, W., Li, Q., Yin, G., Zhang, N., and Cai, W. (2013). Edaravone protects against glutamate-induced PERK/EIF2α/ATF4 integrated stress response and activation of caspase-12. Brain Res. *1519*, 1–8.

Gencic, S., Abuelo, D., Ambler, M., and Hudson, L.D. (1989). Pelizaeus-Merzbacher disease: an X-linked neurologic disorder of myelin metabolism with a novel mutation in the gene encoding proteolipid protein. Am. J. Hum. Genet. *45*, 435–442.

Gow, A., and Lazzarini, R.A. (1996). A cellular mechanism governing the severity of Pelizaeus-Merzbacher disease. Nat. Genet. *13*, 422–428.

Gow, A., Friedrich, V.L., Jr., and Lazzarini, R.A. (1994). Many naturally occurring mutations of myelin proteolipid protein impair its intracellular transport. J. Neurosci. Res. *37*, 574–583.

Gow, A., Gragerov, A., Gard, A., Colman, D.R., and Lazzarini, R.A. (1997). Conservation of topology, but not conformation, of the proteolipid proteins of the myelin sheath. J. Neurosci. *17*, 181–189.

Gow, A., Southwood, C.M., and Lazzarini, R.A. (1998). Disrupted proteolipid protein trafficking results in oligodendrocyte apoptosis

in an animal model of Pelizaeus-Merzbacher disease. J. Cell Biol. *140*, 925–934.

Griffiths, I., Klugmann, M., Anderson, T., Yool, D., Thomson, C., Schwab, M.H., Schneider, A., Zimmermann, F., McCulloch, M., Nadon, N., and Nave, K.A. (1998). Axonal swellings and degeneration in mice lacking the major proteolipid of myelin. Science *280*, 1610–1613.

Hodes, M.E., Aydanian, A., Dlouhy, S.R., Whelan, D.T., Heshka, T., and Ronen, G. (1998). A de novo mutation (C755T; Ser252Phe) in exon 6 of the proteolipid protein gene responsible for Pelizaeus-Merzbacher disease. Clin. Genet. *54*, 248–249.

Hu, B.Y., Du, Z.W., and Zhang, S.C. (2009). Differentiation of human oligodendrocytes from pluripotent stem cells. Nat. Protoc. *4*, 1614–1622.

Imaizumi, Y., Okada, Y., Akamatsu, W., Koike, M., Kuzumaki, N., Hayakawa, H., Nihira, T., Kobayashi, T., Ohyama, M., Sato, S., et al. (2012). Mitochondrial dysfunction associated with increased oxidative stress and α-synuclein accumulation in PARK2 iPSC-derived neurons and postmortem brain tissue. Mol. Brain *5*, 35.

Izrael, M., Zhang, P., Kaufman, R., Shinder, V., Ella, R., Amit, M., Itskovitz-Eldor, J., Chebath, J., and Revel, M. (2007). Human oligodendrocytes derived from embryonic stem cells: Effect of noggin on phenotypic differentiation in vitro and on myelination in vivo. Mol. Cell. Neurosci. *34*, 310–323.

Kang, S.M., Cho, M.S., Seo, H., Yoon, C.J., Oh, S.K., Choi, Y.M., and Kim, D.W. (2007). Efficient induction of oligodendrocytes from human embryonic stem cells. Stem Cells *25*, 419–424.

Lim, M.P., Devi, L.A., and Rozenfeld, R. (2011). Cannabidiol causes activated hepatic stellate cell death through a mechanism of endoplasmic reticulum stress-induced apoptosis. Cell Death Dis. *2*, e170.

Mikoshiba, K., Okano, H., Tamura, T., and Ikenaka, K. (1991). Structure and function of myelin protein genes. Annu. Rev. Neurosci. *14*, 201–217.

Nori, S., Okada, Y., Yasuda, A., Tsuji, O., Takahashi, Y., Kobayashi, Y., Fujiyoshi, K., Koike, M., Uchiyama, Y., Ikeda, E., et al. (2011). Grafted human-induced pluripotent stem-cell-derived neurospheres promote motor functional recovery after spinal cord injury in mice. Proc. Natl. Acad. Sci. USA *108*, 16825–16830.

Ohta, S., Imaizumi, Y., Okada, Y., Akamatsu, W., Kuwahara, R., Ohyama, M., Amagai, M., Matsuzaki, Y., Yamanaka, S., Okano, H., and Kawakami, Y. (2011). Generation of human melanocytes from induced pluripotent stem cells. PLoS ONE *6*, e16182.

Okada, Y., Shimazaki, T., Sobue, G., and Okano, H. (2004). Retinoic-acid-concentration-dependent acquisition of neural cell identity during in vitro differentiation of mouse embryonic stem cells. Dev. Biol. *275*, 124–142.

Okada, Y., Matsumoto, A., Shimazaki, T., Enoki, R., Koizumi, A., Ishii, S., Itoyama, Y., Sobue, G., and Okano, H. (2008). Spatiotemporal recapitulation of central nervous system development by murine embryonic stem cell-derived neural stem/progenitor cells. Stem Cells *26*, 3086–3098.

Seitelberger, F. (1995). Neuropathology and genetics of Pelizaeus-Merzbacher disease. Brain Pathol. *5*, 267–273.

Shimada, H., Okada, Y., Ibata, K., Ebise, H., Ota, S., Tomioka, I., Nomura, T., Maeda, T., Kohda, K., Yuzaki, M., et al. (2012). Efficient derivation of multipotent neural stem/progenitor cells from non-human primate embryonic stem cells. PLoS ONE *7*, e49469.

Shimojima, K., Inoue, T., Imai, Y., Arai, Y., Komoike, Y., Sugawara, M., Fujita, T., Ideguchi, H., Yasumoto, S., Kanno, H., et al. (2012). Reduced PLP1 expression in induced pluripotent stem cells derived from a Pelizaeus-Merzbacher disease patient with a partial PLP1 duplication. J. Hum. Genet. *57*, 580–586.

Southwood, C.M., Garbern, J., Jiang, W., and Gow, A. (2002). The unfolded protein response modulates disease severity in Pelizaeus-Merzbacher disease. Neuron *36*, 585–596.

Takahashi, K., Tanabe, K., Ohnuki, M., Narita, M., Ichisaka, T., Tomoda, K., and Yamanaka, S. (2007). Induction of pluripotent stem cells from adult human fibroblasts by defined factors. Cell *131*, 861–872.

Thomson, C.E., Montague, P., Jung, M., Nave, K.A., and Griffiths, I.R. (1997). Phenotypic severity of murine Plp mutants reflects in vivo and in vitro variations in transport of PLP isoproteins. Glia *20*, 322–332.

Wang, S., Bates, J., Li, X., Schanz, S., Chandler-Militello, D., Levine, C., Maherali, N., Studer, L., Hochedlinger, K., Windrem, M., and Goldman, S.A. (2013). Human iPSC-derived oligodendrocyte progenitor cells can myelinate and rescue a mouse model of congenital hypomyelination. Cell Stem Cell *12*, 252–264.

Yin, X., Baek, R.C., Kirschner, D.A., Peterson, A., Fujii, Y., Nave, K.A., Macklin, W.B., and Trapp, B.D. (2006). Evolution of a neuroprotective function of central nervous system myelin. J. Cell Biol. *172*, 469–478.

Yoshida et al. Molecular Brain 2014, 7:45
http://www.molecularbrain.com/content/7/1/45

Molecular Brain

RESEARCH Open Access

The use of induced pluripotent stem cells to reveal pathogenic gene mutations and explore treatments for retinitis pigmentosa

Tetsu Yoshida[1,2†], Yoko Ozawa[1,2*†], Keiichiro Suzuki[3], Kenya Yuki[1,2], Manabu Ohyama[4], Wado Akamatsu[5], Yumi Matsuzaki[5], Shigeto Shimmura[1], Kohnosuke Mitani[3], Kazuo Tsubota[1] and Hideyuki Okano[5*]

Abstract

Background: Retinitis pigmentosa (RP) is an inherited human retinal disorder that causes progressive photoreceptor cell loss, leading to severe vision impairment or blindness. However, no effective therapy has been established to date. Although genetic mutations have been identified, the available clinical data are not always sufficient to elucidate the roles of these mutations in disease pathogenesis, a situation that is partially due to differences in genetic backgrounds.

Results: We generated induced pluripotent stem cells (iPSCs) from an RP patient carrying a *rhodopsin* mutation (E181K). Using helper-dependent adenoviral vector (HDAdV) gene transfer, the mutation was corrected in the patient's iPSCs and also introduced into control iPSCs. The cells were then subjected to retinal differentiation; the resulting rod photoreceptor cells were labeled with an *Nrl* promoter-driven enhanced green fluorescent protein (EGFP)-carrying adenovirus and purified using flow cytometry after 5 weeks of culture. Using this approach, we found a reduced survival rate in the photoreceptor cells with the E181K mutation, which was correlated with the increased expression of endoplasmic reticulum (ER) stress and apoptotic markers. The screening of therapeutic reagents showed that rapamycin, PP242, AICAR, NQDI-1, and salubrinal promoted the survival of the patient's iPSC-derived photoreceptor cells, with a concomitant reduction in markers of ER stress and apoptosis. Additionally, autophagy markers were found to be correlated with ER stress, suggesting that autophagy was reduced by suppressing ER stress-induced apoptotic changes.

Conclusion: The use of RP patient-derived iPSCs combined with genome editing provided a versatile cellular system with which to define the roles of genetic mutations in isogenic iPSCs with or without mutation and also provided a system that can be used to explore candidate therapeutic approaches.

Keywords: iPS cells, Retina, Neurodegeneration, Gene delivery, Drug screening, ER stress

Background

Recent advances in molecular genetics have enabled the early diagnosis of neurodegenerative diseases, including retinitis pigmentosa (RP), an inherited retinal disorder that causes progressive photoreceptor cell loss and visual function impairment that can limit social activity and the ability to work. Despite its early detection, there is currently no cure for this disease.

Approximately 3,000 mutations have been reported in 50 genes in RP patients [1], and more than 100 point mutations have been identified in the *rhodopsin* gene [2]. Rhodopsin, an evolutionarily conserved seven-transmembrane protein specifically produced in photoreceptor cells, is first localized to the endoplasmic reticulum (ER) and is then transported to the outer segment discs where it responds to photon activation via conformational changes. Pathological responses to genetic mutations in *rhodopsin* typically occur in an autosomal dominant manner due to the production of an abnormal protein. Some

* Correspondence: ozawa@a5.keio.jp; hidokano@a2.keio.jp
†Equal contributors
[1]Laboratory of Retinal Cell Biology, Department of Ophthalmology, Keio University School of Medicine, 35 Shinanomachi, Shinjuku-ku 160-8582, Tokyo, Japan
[5]Department of Physiology, Keio University School of Medicine, 35 Shinanomachi, Shinjuku-ku 160-8582, Tokyo, Japan
Full list of author information is available at the end of the article